Ore Geology Reviews 64 (2015) 354–386

Contents lists available at ScienceDirect

Ore Geology Reviews

journal homepage: www.elsevier.com/locate/oregeorev

Structural controls on the primary distribution of mafic–ultramafic intrusions containing Ni–Cu–Co–(PGE) sulfide mineralization in the roots of large igneous provinces

Peter C. Lightfoot [a], Dawn Evans-Lamswood [b]

[a] Vale, Exploration, Highway 17 West, Sudbury, Ontario P0M 1N0, Canada
[b] Vale Newfoundland and Labrador Limited, 10 Fort William Place, Baine Johnston Centre, Suite 700, St. John's, Newfoundland, A1C 1K, Canada

ARTICLE INFO

Article history:
Received 27 May 2014
Received in revised form 15 July 2014
Accepted 17 July 2014
Available online 27 July 2014

Keywords:
Small mafic–ultramafic intrusions
Nickel sulfide deposits
Chonolith
Transtension
Strike-slip
Emplacement of magmatic sulfide

ABSTRACT

Deposits of Ni–Cu–Co–(PGE) sulfide often occur in association with small differentiated intrusions that reside within local transtensional spaces in strike-slip fault zones. These faults often develop in response to incipient rifting of the crust and the development of large igneous provinces due to far-field stresses generated by plume-induced continental drift. We review the geology of a number of large and small nickel sulfide deposits and the associated intrusions, and show that the geometry of the host intrusion and localization of the mineral zones can be classified into three main groups. Further, we show that the morphology of each is controlled by space created in response to deformation on structures.

One group of intrusions has the plan shape of an asymmetric rhomboid with the long axis sub-parallel to a fault zone, and contacts which have often been structurally modified during and/or after emplacement of the magma. The typical cross section is a downward-closing cone shape with curved walls and often a dyke-like keel at the base. This morphology is found in the Ovoid and Discovery Hill Zones of the Voisey's Bay Deposit (Canada), the Jinchuan, Huangshan, Huangshandong, Hongqiling, Limahe, Qingquanshan, and Jingbulake (Qingbulake) Intrusions in China, and the Eagle and Eagle's Nest deposits in the USA and Canada, respectively.

A second group of deposits is associated with conduits within dyke and sheet-like intrusions; these deposits are often associated with discontinuities in the dyke which were created in response to structural controls during emplacement. Examples include the Discovery Hill Deposit and the Reid Brook Zone of the Voisey's Bay Intrusion, where there are plunging domains of thicker dyke which control the mineralization inside the dyke, and thin discontinuous segments of the dyke which are associated with structurally controlled mineralization in the surrounding country rock gneisses. The Oktyabrysk, Taimyrsk, Komsomolsk, and Gluboky Deposits in the Noril'sk Region of Russia are localized at the base of thicker parts of the Kharaelakh Intrusion which appear to be a conduit that follows synformal features in the country rocks located west of the Noril'sk–Kharaelakh Fault. Other examples of dyke-like bodies with both variation in width and the development of discontinuities are the Copper Cliff and Worthington Offset Dykes which radiate away from the Sudbury Igneous Complex (Canada). The distribution of ore bodies in these Sudbury Offset Dykes is principally controlled by variations in the thickness of the dyke, interpreted to reflect the presence of conduits within the dyke.

A third group of mineralized intrusions located within structural corridors have the geometry of oblate tubes; examples include Kalatongke in China, Northeastern Talnakh and Noril'sk 1 in Russia, Babel–Nebo in Australia, and Nkomati in South Africa. Sometimes these oblate tube-like intrusions form in bridging structures between larger intrusions hosted in the more significant structures. Examples include the Tamarack Intrusion in Minnesota, USA, and the Current Lake Complex in Ontario, Canada, both of which contain magmatic Ni–Cu sulfide mineralization.

In all of these deposits, the intrusions appear to be open system magma pathways, and so the term “chonolith” can be applied to describe them as a group. All of these intrusions are characterized by a high ratio of sulfide/silicate; there are 1–3 orders of magnitude more sulfide in the intrusion than the magma contained in the intrusion is capable of dissolving. The formation of these deposits is considered to have taken place in open system magma conduits. It is possible that the metal tenor of the sulfides were upgraded by equilibration of successive batches of silicate magma passing through the conduit, and equilibrating with a stationary pool of magmatic sulfide. At Voisey's Bay there appears little doubt that the sulfides were injected through a conduit dyke into higher level magma chambers. A similar model has been proposed for the formation of the deposits at Jinchuan and Noril'sk–Kharaelakh. Economically significant nickel sulfide deposits that tend to be high in Ni tenor, are often related to the late injection of magma that form distinct parts of the intrusion, and the localization of mineralization tends to be related to changes in the geometry of the magma chamber. Strongly deformed and metamorphosed komatiite-associated deposits (e.g. Pechenga, Thompson, and the Yilgarn komatiite associations)

http://dx.doi.org/10.1016/j.oregeorev.2014.07.010

appear to be the remains of open system magma conduits which are now represented by segmented and boudinaged ultramafic bodies as a result of more than 4 phases of post-emplacement deformation.
LIP activity at craton margins has long been recognized as a key control on the genesis of magmatic sulfide deposits; we show that the principal regional controls of strike-slip tectonics underpin the local geometry of the intrusions, and we provide an explanation for why so many of the global nickel sulfide ore deposits are associated with intrusions that share common morphologies and characteristics. This model provides a framework for more detailed structural investigations of nickel sulfide deposits, and it is a predictive framework for mineral exploration.

1 . Introduction

The principal geological controls on the formation and localization of magmatic Ni–Cu–Co–platinum group element (PGE) sulfide mineralization have been widely discussed (e.g. Barnes and Lightfoot, 2005; Keays, 1995; Lightfoot, 2007; Naldrett 2004, 2010). It is now generally accepted that the formation of economic concentrations of mineralization requires: 1. A primitive S-undersaturated and metal un-depleted parental magma originating from the mantle; 2. a sulfide saturation event that produced a dense immiscible magmatic sulfide (e.g. Keays and Lightfoot, 2009); 3. enrichment of the sulfides in metals by equilibration of the sulfide magma with a large relative amount of silicate melt; and 4. accumulation and localization of the dense sulfide melt into traps at the margin of the intrusion that contains the mineralization (e.g. Keays, 1995; Lightfoot, 2007; Naldrett 2004, 2010 and references therein). The compositions of these sulfide melts can be modified by processes which fall into two broad groups: 1. Fractional crystallization of the magmatic sulfide to produce a Cu-rich liquid and a monosulfide solid solution (Keays and Crocket, 1970); and 2. modification by post-magmatic processes that remobilize and fractionate the sulfides during deformation, metamorphism, and hydrothermal activity (Farrow and Watkinson, 1997; Lightfoot et al., 2012a,b).

Although much attention has been paid to the petrology and geochemistry of the sulfide-bearing rocks and the magmatic processes responsible for their formation (Barnes and Lightfoot, 2005; Naldrett, 2004, 2010), less attention has been paid to the morphology of the magma chambers and conduits that form the intrusions which contain these sulfides (Ripley and Li, 2011). This paper reports evidence to suggest that mafic–ultramafic intrusions that contain Ni–Cu–Co–(PGE) sulfide mineralization share several key features which make them part of a group, viz: 1. The relative volumes of sulfide to silicate magma in the intrusions is high and the metal content of these sulfides is also very high, thus, these sulfides cannot have formed by in-situ segregation and accumulation from the observed volume of silicate magma contained in the intrusion (e.g. Naldrett et al., 1995); 2. the internal distribution of rock types is complex and includes a range of rock types from ultramafic through mafic as well as local development of magmatic breccias that are typically spatially associated with the sulfide mineralization (e.g. Lightfoot, 2007); 3. the intrusions have morphologies that are controlled by pre-existing and reactivated structures in the crust that guided magma from the mantle to shallower levels (e.g. Lightfoot et al., 2012a); and 4. there is now strong evidence to suggest that sulfides were injected as sulfide- and fragment-laden magmas and possibly sulfide magma into a final resting place (Lightfoot et al., 2012a,b; Tang, 1992, 1993).

This study reports a review of key aspects of a group of Ni–Cu–Co–(PGE) deposits found in China; these include Mesozoic deposits associated with intrusions cutting largely Carboniferous-aged country rocks in the Kangguer Fault Zone of eastern Xinjiang (deposits associated with intrusions at Huangshan, Huangshandong, Hulu, Tulargen, Erhongwa, and Xianshan), the Nalatishan Fault Zone in western Xinjiang (Jingulake), the Fuyun Fault Zone of northern Xinjiang (Kalatongke), the Longshoushan Fault Zone of Gansu Province (Jinchuan), the Huifeihe Fault Zone of Jilin Province (Hongqiling), and the North–South Panxi Region faults in the roots of the Permian-aged Emeishan flood basalts of Yunnan and Sichuan Provinces (Yangliuping, Limahe, Qingquanshan, Baimazhai, Jinbaosan). We show how this model is important in understanding the origin of the deposits at Noril'sk–Talnakh and Voisey's Bay. The global significance is then emphasized with reference to other deposits which also share these features; these include Babel–Nebo Western Australia), Nkomati (South Africa), Eagle, Tamarack, and Current Lake (Mid-continent Rift of Canada and the USA), and Double Eagle (Ontario, Canada). We show how these intrusions are all part of a group of open system magma channels or conduits which have traditionally been termed chonoliths (e.g. Naldrett et al., 1995), and we show how these intrusions develop in localized open space created by cross-linking structures within major strike-slip fault zones towards the margins of cratonic bodies. We propose that the entire class of deposits form in a direct response to the plumbing system in structural zones where magma migration is controlled by a process of tectonic pumping which transfers both sulfide and crystal-laden magmas through open system passageways. The geological setting in which these systems were developed relates to supercontinent break-up, and large igneous province (LIP) magmatism at cratonic margins (e.g. Begg et al., 2010).

2 . Geology of the Chinese nickel deposits

The distribution of nickel sulfide deposits in China is summarized in Fig. 1, where the size of the symbol is proportional to the original Ni content of the deposit (modified after Tang, 1992). The deposits range in age from Phanerozoic to Mesozoic and although the tectonic setting tends to be associated with the cratonic margin, some of the deposits link to large igneous province events whereas others occur in structural corridors within late orogenic belts (e.g. Zhou et al., 2002). The Jinchuan Intrusion and deposits are part of the Neoproterozoic Rodinian plume event (Pirajno, 2012; Fig. 1). The intrusions associated with the early Permian Tarim LIP include those hosting the deposits of the Kangguer Fault Zone in the Huangshan-Jing'erquan area (Figs. 1 and 2A). The Panxi faults in the roots of the Emeishan LIP contain a number of deposits like Limahe and Yangliuping (Pirajno, 2012). Some mineralized intrusions pre-date the Early Permian LIP by up to 200 Ma; an example is the Jingbulake Intrusion in the Nalatishan Fault Zone in the Western Tian Shan area. Intrusions developed in structures cutting the Central Asian Orogenic Belt appear to belong to a Mesozoic igneous event as recorded by the 217 Ma age of the Hongqiling Intrusion (Wu et al., 2004). A summary of relevant geological features of each of the deposits is given in Table 1.

2.1. The Huangshan-Jing'erquan Belt intrusions and nickel deposits of the Kangguer Fault Zone, eastern Xinjiang

The Huangshan-Jing'erquan Belt contains the second largest combined resource of nickel sulfide in China (Mao et al., 2008). The majority of the deposits occur along the Kangguer strike-slip fault system in the eastern segment of the Tian Shan Belt of the Central Asian Orogen. Fig. 2A shows the geology of northwestern China, and highlights the distribution of the deposits in the context of regional strike-slip faults identified by Cunningham and Mann (2007) based on the digital elevation model for the region and structural work referenced in these papers.

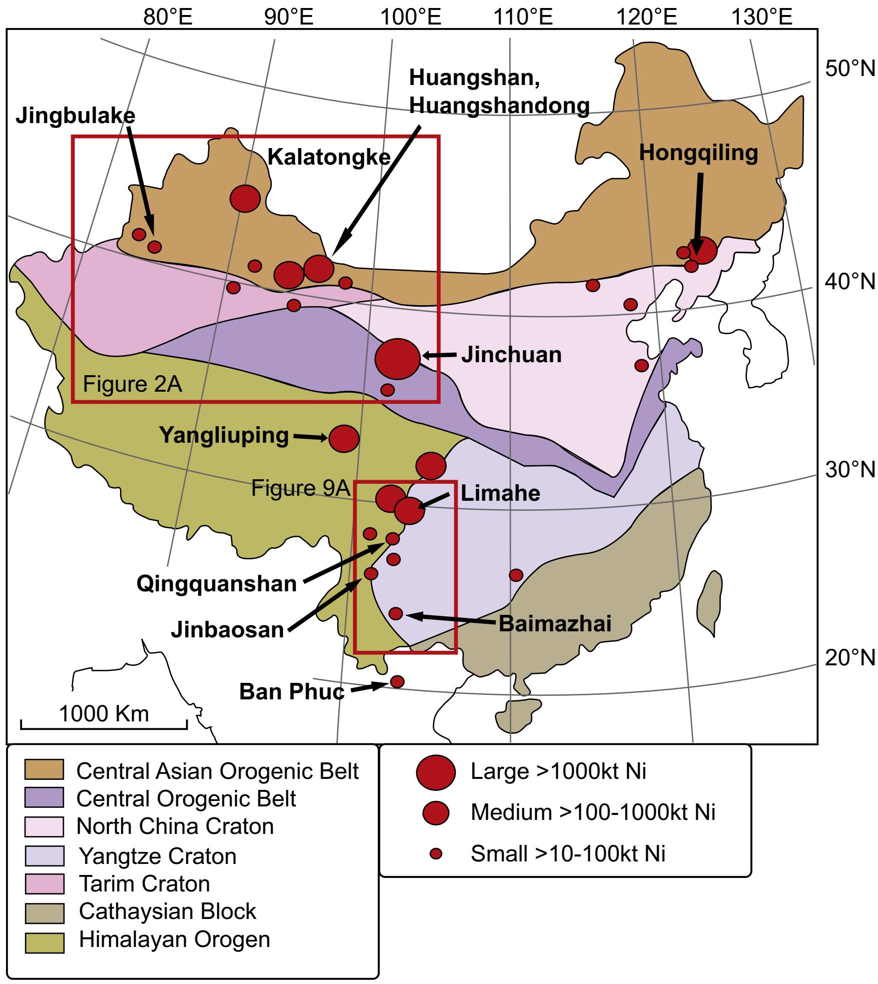

Fig. 1. Geological map of China simplified to show major terrains and shield areas. The distribution and size of Ni sulfide deposits are shown.

The clearest examples of strike-slip motion are evident in the area of the Hami (Turpan) Basin on the regional scale digital elevation model (Fig. 2B), where the Boghda, Al Bogd, and Barkoi Tagh mountain ranges to the north are transpressional sigmoidal-shaped positive flower structures. The Hami Basin to the south is a negative flower structure produced by large cross-linking structures in the strike-slip structure (Mann, 2007). The area of significance with respect to the mineralized intrusions of the Huangshan-Jing'erquan Belt is located south and east of the Hami Basin, and this is an area with a subsidiary fault system including the Kangguer, Huangshan, and Gandun Faults which collectively comprise a structural corridor which has a dark maroon color anomaly on the enhanced Landsat image in Fig. 2C. Intrusions in this sinistral transcurrent fault zone include a number of granodiorite bodies that have an elongated rhomboid shape (white rhomboids in Fig. 2C) with the long axis of the rhomboid sub-parallel to the fabric (see also Wang et al., 2014). There are also a number of mafic–ultramafic intrusions in this belt which are typically much smaller in size (~0.5–5 km), also with their long axes sub-parallel to the fault.

The 2.8 km^2 Huangshandong Intrusion is the largest in the belt, and it comprises a 268 Ma (Zhou et al., 2002) series of pyroxenites, olivine gabbros, gabbros and diorites which form a broadly zoned body with a rhomboid shape in plan and a cone shape in the north–south cross section as shown in Fig. 3A–B (Wang et al., 1987). The disseminated pyrrhotite–pentlandite–chalcopyrite mineralization is localized as stratiform accumulations in the more primitive rocks. The contact zones of the Huangshandong Intrusion are typically structurally modified and now comprised of weakly foliated dioritic rocks. The intrusion fills a transtensional space created by sinsitral movement on a left-stepping fault. The rhomboid geometry is a result of the left-stepping fault displacement and the cross-linking fault structures (e.g. Mann, 2007).

The Huangshan Intrusion is within the Kangguer Fault System (Fig. 2A) and has a broadly similar range of rock types and style of mineralization to Huangshandong (Fig. 4A–C) and Jinchuan (Fig. 5A–D). The intrusion consists of dunite, peridotite, websterite, gabbronorite, gabbro and diorite. The mineralization is largely contained within the more primitive rocks within the keel of the intrusion. The marginal rocks of the intrusion are typically variably sheared gabbronorites in structural contact with siltstones and basalts. The intrusion curves into the fault on the south side, and extends along the fault on the north side. The intrusion appears to fill a space in a cross-linking structure produced by sinistral movement in the Kangguer Fault Zone (Mann, 2007).

The Erhongwa Intrusion and the Xianshan, Hulu, and Tulargen intrusions, which are associated with other small intrusions rest within the Kangguer Fault system zone (e.g. Mao et al., 2008; Shen et al., 2008; Sun et al., 2013; Wang et al., 1987), and although much of the detail of the internal geometry of the deposits is not yet published, the geometry of these intrusions provides similar examples to Huangshan and Hunagshandong where small intrusive bodies filled spaces created by local transtension in cross-linking structures as a result of displacement along the Kangguer strike-slip fault zone.

2.2. The Jinchuan Deposit, Longshoushan Fault Zone, Gansu Province

The largest deposit in central western China is Jinchuan which contained an original resource of approximately 5000 kt Ni in

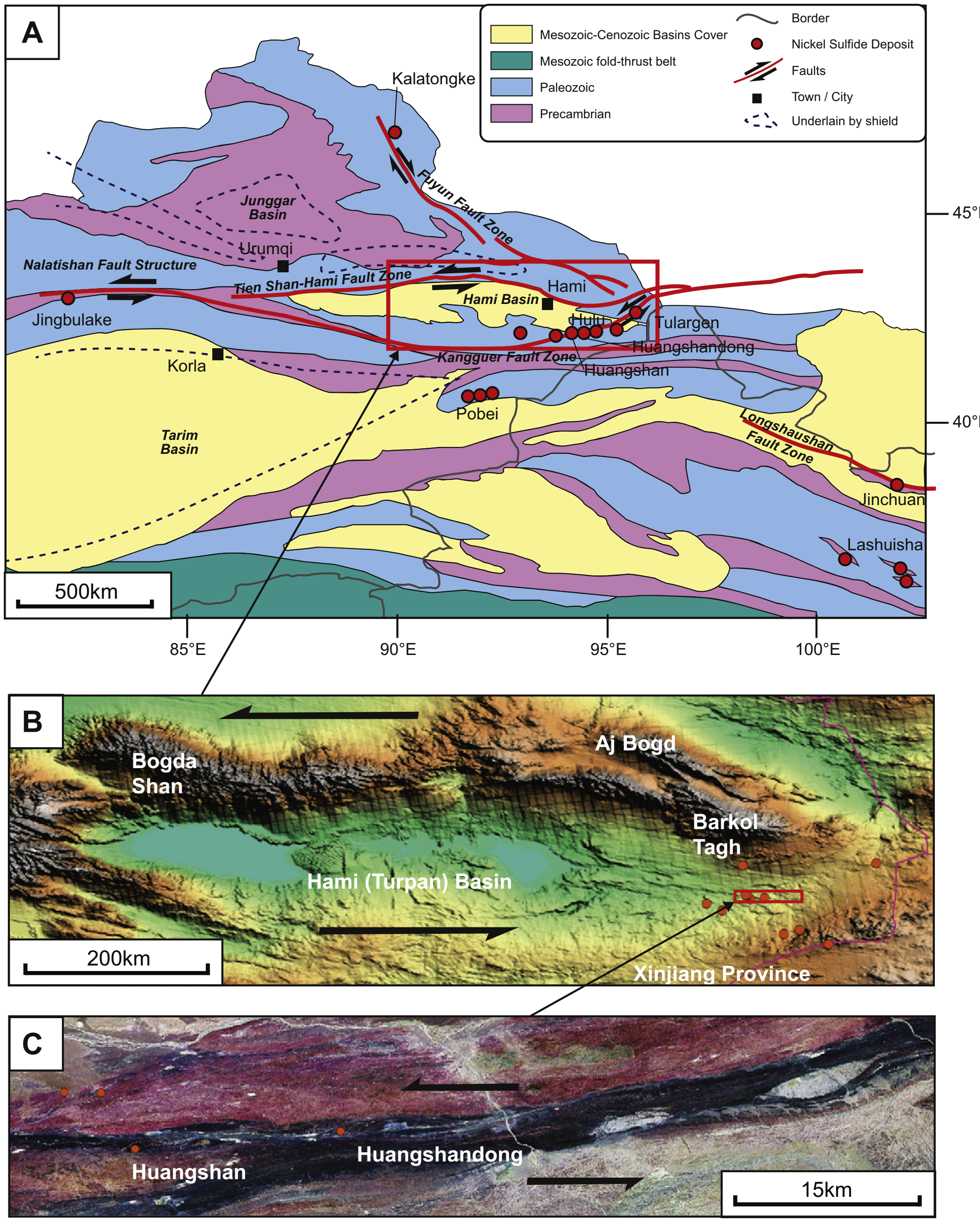

Fig. 2. A. Geological map of Western China showing the principal geological units and the location of major strike-slip structural zones (after Tang, 1992). B. Digital terrain model of eastern Xinjiang in the area of the Hami Basin showing the major mountain ranges in areas of transpression, and basins in areas of transtension (modified after Mann, 2007). C. Landsat image enhanced to show the distribution of carboniferous host rocks (purple), granitoid rocks (white) and mafic–ultramafic intrusions at Huangshan and Huangshandong.

association with ultramafic rocks of the host intrusion. The intrusion is located in a Proterozoic Belt termed the Longshushan, and is dissected by the Longshoushan Fault Zone which is aligned parallel to the long axis of the Belt (Fig. 2). The geology of the intrusion and distribution of mineralization have been reported in Tang (1993), and a synthesis of the geology in plan and three representative cross sections is shown in Fig. 5A–D. The intrusion has a surface area of < 1.5 km^2, and extends to a depth of at least 2 km as a dyke-like stem or narrow cone-shaped keel in cross section. The geometry of the intrusion is similar to that previously described at Huangshandong. The Jinchuan intrusion comprises four segments of different thickness that are cut by late NE–SW faults. The mineralization in Number 1 Mine Area in the west outcropped at surface where the original discovery was made, however the mineralization in Number 2 Mine Area is entirely at depth within the intrusion, and the lherzolite, plagioclase lherzolite, and dunite at the surface are devoid of disseminated sulfide mineralization. The margins of the intrusion are variously described as serpentinized dunite and lherzolite through to pyroxenite. The vast majority of the contacts are complicated by structures which appear to not only have had late motion, but may be part of a regional network of structures that controlled the emplacement of the Jinchuan magma at 827 +/− 8 Ma (Li et al., 2004) and were probably related to the break-up of Rodinia (Pirajno, 2012). Limited published data and a complex deformation history of the Longshoushan Belt do not provide clear kinematic indicators for Jinchuan or the sense of displacement of the structures. However, the form of the intrusion and internal distribution of rocks types shown in

Table 1
Summary of geological features of small intrusions with nickel sulfide mineralization developed within or adjacent to structures.

Intrusion name	Deposit name	Location	Age of intrusion	Igneous event	Major structure	Morphology	Rock types associated with mineralisation	Barren rock types
Huangshan	Huangshan	Xinjiang Region, China	269 +/− 2 Ma	Tarim LIP	Kanguer Fault Zone	Elongate rhomb with cross section of curved cone that bends into the fault zone at the SW termination	Dunite, peridotite, websterite, hornblende peridotite	Gabbronorite, gabbro, diorite
Huangshandong	Huangshandong	Xinjiang Region, China	282 +/− 20 Ma	Tarim LIP	Kanguer Fault Zone	Elongate rhomb with cross section of curved cone that narrows into the structure at each end	Peridotite, gabbronorite	Gabbro, diorite
Xiangshan	Xiangshan	Xinjiang Region, China	285 +/− 1.2 Ma	Tarim LIP	Kanguer Fault Zone	Elongate rhomb with cross section of curved cone that narrows into the structure at each end	Peridotite, gabbronorite	Gabbro, diorite
Hulu	Hulu	Xinjiang Region, China	282.3 +/1.2 Ma	Tarim LIP	Kanguer Fault Zone	Trough with possible feeder dyke	Websterite	Websterite, peridotite, gabbro
Tulargen	Tulargen	Xinjiang Region, China	301 +/− 3 Ma	Tarim LIP	Kanguer Fault Zone	Dyke-like body	Gabbro and hornblende olivine gabbro	Gabbro
Kalatongke	Kalatongke	Xinjiang Region, China	287 +/− 5 Ma	Tarim LIP	Fuyun Fault Zone	Weakly elongate rhomb in surface plan with eliptical cross section	Hornblende gabbro, pyroxenite, and biotite gabbro	Gabbro and diorite
Jingbulake (Qingbulake)	Jingbulake	Xinjiang Region, China	454 Ma	Altaid LIP	Nalatishan Fault Zone	Elongate rhomb with cross section of curved cone that narrows into the structure at each end	Olivine gabbro, peridotite and hornblende gabbro	Olivine gabbro, pyroxenite, hornblende gabbro and diorite
Jinchuan	Jinchuan	Gansu Province, China	827 +/− 8 Ma	Proterozoic Longshoushan Belt	Longshoushan fault zone	Segmented elongated rhomb with a narrow cone-shaped or sheet-like cross section	Dunite	Lherzolite and plagioclase lherzolite
Jilin #1	Hongqiling	Jilin Province, China	217 Ma	Altaid event	Huifeiheg fault zone	Elongate rhomb with cross section of curved cone that narrows into the structure at each end	Olivine pyroxenite and pyroxenite	Gabbro
Jilin #7	Hongqiling	Jilin Province, China	217 Ma	Altaid event	Huifeiheg fault zone	Sheet-like dyke narrowing into structure	Orthopyroxenite	Orthopyroxenite
Limahae	Limahae	Sichuan Province, China	263 +/− 3 Ma	Altaid event	Panxi Fault Zone	Elongate rhomb with cross section of curved cone that narrows into the structure at each end and an asymmetric dyke-like keel	Pyroxenite and peridotite	Gabbro and diorite
Qingquanshan	Qingquanshan	Sichuan Province, China		Emeishan LIP	Panxi Fault Zone	Elongate rhomb with cross section of curved cone that narrows into the structure at each end	Peridotite, gabbronorite	Gabbro
Baimazhai	Baimazhai	Yunnan Province, China	258.5 +/ − 3.5 Ma	Emeishan LIP	Red River Fault Zone	U-shaped tube	Olivine pyroxenite and peridotite	Gabbro
Kharaelakh	Oktyabrysk, Komsomlsk, Myak, Taimysk, Gluboky	Noril'sk Region, Siberia, Russia		Siberian LIP	Noril'sk–Kharaelakh Fault	Undulating sheet with thicker channel-ways	Taxite, olvine gabbrodolerite, picritic gabbrodolerite	Olivine gabbro, gabbro, leucogabbro
Talnakh	Komsomolsk, Skalisty, Severny	Noril'sk Region, Siberia, Russia		Siberian LIP	Noril'sk–Kharaelakh Fault	Undulating sheet with thicker channel-ways	Taxite, olvine gabbrodolerite, picritic gabbrodolerite	Olivine gabbro, gabbro, leucogabbro
Noril'sk 1	Medvehy Ruchi and Zapolyarny	Noril'sk Region, Siberia, Russia	251.2 +/-0.3 Ma (290 +/− 2.8 to 226 +/ − 0.9 Ma)*	Siberian LIP	Noril'sk–Kharaelakh Fault	Undulating sheet with thicker channel-ways	Taxite, olvine gabbrodolerite, picritic gabbrodolerite	Olivine gabbro, gabbro, leucogabbro

Parental magma	Country rocks and Sulfur source	Magmatic breccias	Sulfide type	Sulfide assemblage	Surface area (or projected surface area of cross section of intrusion) km2	Ratio of barren intrusive rock to mineralized intrusive rock	Typical Ni100 wt.%	Typical 3E100 g/t	References
Tholeiite and high-Mg tholeiite	Lower Carboniferous Gandun Group turbidites with little crustal sulfur	None known	Disseminated with minor massive sulfide	Po >> Cpy > Pn	3	~50	8.5	1	Wang et al. (1987);Mao et al. (2008); Shen et al. (2008)
Tholeiite and high-Mg tholeiite	Lower Carboniferous Gandun Group turbidites with little crustal sulfur	None known	Disseminated	Po >> Cpy > Pn	5	~50	6	0.1	Wang et al. (1987);Mao et al. (2008); Shen et al. (2008)
Tholeiite and high-Mg tholeiite	Lower Carboniferous Wutongwozi Formation volcanic rocks	None known	Disseminated	Po >> Cpy > Pn	12	~50	5	0.25	Wang et al. (1987);Mao et al. (2008); Shen et al. (2008)
Tholeiite and high-Mg tholeiite	Lower Carboniferous Wutongwozi Formation volcanic rocks	None known	Disseminated	Po >> Cpy > Pn	0.5	~50	6	0.5	Mao et al. (2008); Shen et al. (2008); Han et al. (2013)
Tholeiite and high-Mg tholeiite	Carboniferous Tudun Formation volcanic rocks with no crustal sulfur	None known	Disseminated, net-textured and semi-massive sulfide	Po >> Cpy > Pn	0.25	~2	5	0.25	Mao et al. (2008)
Tholeiitic	Carboniferous Nanmingshu Formation clastic rocks; no sulfur	None know	Disseminated with subordinate massive sulfide	Po > Cpy > Pn > Cub	0.25	~5	3.5	3	Wang et al. (1992), Wang et al. (1991), Mao et al. (2008), Gao et al. (2012).
Tholeiite and high-Mg tholeiite	Gneiss devoid of crustal sulfur	None known	Disseminated sulfide	Po > Cpy > Pn > Cub	3	~100	11	0.13	Yang et al. (2012), Zhang et al. (2006), Mao et al. (2008)
High-Mg tholeiite	Proterozoic granitoids, gneisses, and marbles devoid of significant crustal sulfur	None known	Disseminated and net-textured with rare massive sulfide	Po > Pn> > Cpy	1.4	~10	11.5	0.2	Tang (1993); Li et al. (2004)
High-Mg tholeitte	Hulan Group metasediments devoid of crustal sulfur	None known	Disseminated and net-textured with rare massive sulfide	Po > Pn> > Cpy	0.25	~2	13	0.6	Wu et al. (2004); Lü et al. (2011), Wei et al. (2013)
High-Mg tholeitte	Hulan Group schists and marblers devoid of crustal sulfur	None known	Massive sulfide and disseminated sulfide	Po > Pn> > Cpy	0.1	~1	12	<0.2	Wu et al. (2004); Lü et al. (2011)Wei et al. (2013)
Tholeiite and high-Mg tholeiite	Huli Group limestones and quartzites devoid of crustal sulfur	None known	Massive through to disseminated sulfide	Po > Cpy > Pn > Cub	0.25	~5	8	1	Zhou et al. (2002, 2005)
Tholeiite and high-Mg tholeiite	Hekou Formation carbonate rocks devoid of crustal sulfur	None known	Massive through to disseminated sulfide	Po > Cpy > Pn > Cub	0.05	~2	5	4	
Moderate MgO tholeiite	Ordovician and Devonian clastic sedimentary rocks–shales with minor sulfide content	None known	Massive and disseminated	Po >> Cpy > Pn	0.15	~5	n/a	n/a	(Pu et al., 2007; Tang, 1993; Wang et al., 2006)
Moderate MgO tholeiite	Ravednochinsky shale	Taxites developed	Massive Ni-rich, Cu-prous (upper exocontact), and disseminated (blebby and ragged)	Po > Cpy > Pn > Cub	9	~5	3.8 massive	10 massive	(Hawkesworth et al., 1995; Naldrett, 2004; Naldrett et al., 1992, 1995)
Moderate MgO tholeiite	Ravednochinsky shale	Inclusions of metasediment in taxites	Massive Ni-rich, Cu-prous (lower exocontact), and disseminated (blebby and ragged)	Po > Cpy > Pn > Cub	3	~5	4.9 massive; 5.9 disseminated	17 massive; 42 disseminated	Naldrett et al. (1992, 1995); Hawkesworth et al. (1995); Kamo et al. (2003); Naldrett (2004)
Moderate MgO tholeiite	Tunguska shale	Taxites developed	Disseminated blebby to ragged with minor massive sulfide veins	Po > Cpy > Pn > Cub	15	~5	6.9 massive; 8.3 disseminated	50 massive; 130 disseminated	Kamo et al. (2003), * = Malitch et al. (2012); Naldrett (2004)

(continued on next page)

Table 1 (*continued*)

Intrusion name	Deposit name	Location	Age of intrusion	Igneous event	Major structure	Morphology	Rock types associated with mineralisation	Barren rock types
Voisey's Bay	Ovoid	Labrador, Canada	1334 Ma	Nain Plutonic Suite	VB-Gardar Fault Zone	Bowel-shaped with asymmetric dyke(s?) connected to base	Troctolite, olivine gabbro, variable troctolite, leopard troctolite	Ferrogabbro, normal textured troctolite, olivine gabbro, leucogabbro
Voisey's Bay	Eastern Deeps	Labrador, Canada	1334 Ma	Nain Plutonic Suite	VB-Gardar Fault Zone	Chamber with conduit entry point on north wall plunging towards east	Troctolite, olivine gabbro, variable troctolite, leopard troctolite	Ferrogabbro, normal etxtured troctolite, olivine gabbro, leucogabbro
Voisey's Bay	Reid Brook Zone	Labrador, Canada	1334 Ma	Nain Plutonic Suite	VB-Gardar Fault Zone	Dyke with widened channel-ways and discontinuities plunging ~45° east	Troctolite, olivine gabbro, variable troctolite, leopard troctolite	Ferrogabbro, normal etxtured troctolite, olivine gabbro, leucogabbro
Copper Cliff Deposits	Copper Cliff Offset	Sudbury, Canada	1850 Ma	Sudbury Igneous Complex	Possible radial structural path	Dyke with widened sections that plunge sub-vertically down the dyke axis	Quartz diorite with inclusions	Quartz diorite
Totten	Worthington Offset	Sudbury, Canada	1850 Ma	Sudbury Igneous Complex	Possible radial structural path	Dyke with widened channel-ways and discontinuities plunging ~45° southwest	Quartz diorite with inclusions	Quartz diorite
Babel–Nebo	Babel–Nebo	Musgrave Block, Western Australia	1078 Ma	West Musgrave LIP	No information about possible controlling faults	Elongated tube	Gabbronorite and leucogabbronorite	Leucogabbronorite and gabbronorite
Nkomati (Uitkompst)	Nkomati (Uitkompst)	South Africa	2055 Ma	Bushveld	Possible radial structures link to Bushveld Complex	Tubular body with wings in surrounding sedimentary rocks	Harzburgite	Harzburgite and pyroxenite
Eagle	Eagle	Michigan, USA	1107 Ma	Mid-continent Rift	Possible splay of Great Lakes Tectonic Zone	Dyke with narrow funnel shape widening towards surface	Olivine melagabbro, melatroctolite and feldspathic peridotite	Olivine melagabbro, melatroctolite and feldspathic peridotite
Tamarack (Lakeview)	Lakeview	Minnesota, USA	1106 Ma	Mid-continent Rift	Great Lakes Tectonic Zone	Tubular body with variable with in bridging structure	Lherzolite	Gabbronorite
Crystal Lake Gabbro	Great Lakes Nickel	Ontario, Canada	1099.6 +/− 1.2	Mid-continent Rift	Not known	Trough with possible feeder dyke	Pagmatitic gabbro	Norite, olivine norite, anorthosite
Current Lake	Current Lake	Ontario, Canada	1120 +/− 23	Mid-continent Rift	Quetico Fault Zone	Tubular body connecting dykes	Olivine leucogabbro	Diorite
Ban Phuc	Ban Phuc	Vietnam	257.8 +/− 0.5 Ma	Emeishan LIP	Anning and Yimen Faults in Song Da rift	Trough with possible feeder	Dunite	Dunite
Elan and Elka	Voronezh	Russia	2040–2080 Ma	Bushveld - possible detached conduits	Novogo-Orel Rift with Novohoper fault zone	Irregular anastomosing dyke Elka) and plug-like (Elan)	Gabbronorite	Norite
Double Eagle	Eagle's Nest	Ontario, Canada	2734.5 +/− 1.0 Ma	McFaulds Lake area, greenstone belt	None identified as controling the intrusion	Keel structure at the base of a dyke-like chonolith	Lherzolite, harzburgite	Gabbro
Sally Malay (Savannah)	Sally Malay (Savanah)	Halls Creek, Western Australia	1844 +/− 3	Halls Creek Orogen	Possible splays of Ivanhoe Fault system	Trough with feeder dyke	Ultramafic	Olivine gabbro, norite, troctolite, anorthosite

Parental magma	Country rocks and Sulfur source	Magmatic breccias	Sulfide type	Sulfide assemblage	Surface area (or projected surface area of cross section of intrusion) km2	Ratio of barren intrusive rock to mineralized intrusive rock	Typical Ni100 wt.%	Typical 3E100 g/t	References
Tholeiite	Tasiuyak Gneiss with abundant crustal sulfur	Condensed breccias and inclusion-bearing variable troctolite; no inclusions in massive sulfide	Massive sulfide veins; semi-massive breccia sulfides, net-textured sulfides and disseminated	Po > Cpy > Pn > Cub	0.3	~0.05	4.5	0.9	Lightfoot et al. (2012a, 2012b)
Tholeiite	Tasiuyak Gneiss with abundant crustal sulfur	Condensed breccias and inclusion-bearing variable troctolite; no inclusions in massive sulfide	Massive sulfide veins in dyke and country rock gneisses; semi-massive breccia sulfides, net-textured sulfides and disseminated	Po > Cpy > Pn > Cub	>5	~>100	3.5	1	Lightfoot et al. (2012a, 2012b)
Tholeiite	Tasiuyak Gneiss with abundant crustal sulfur	Condensed breccias and inclusion-bearing variable troctolite; no inclusions in massive sulfide	Massive sulfide veins; semi-massive breccia sulfides, net-textured sulfides and disseminated	Po > Cpy > Pn > Cub	0.1	~5	3	0.8	Lightfoot et al. (2012a, 2012b)
Melt sheet quartz diorite	Country rocks are Proterozoic and typically have little crustal sulfur	Common inclusions of country rocks as well as exotic fragments	Massive, inclusion-rich, and disseminated sulfide	Po > Cpy > Pn > Cub	1 (Offset only)	~10 (offset only)	5.3 to 6.5	12 to 20	Farrow and Lightfoot (2000)
Melt sheet quartz diorite	Country rocks are Proterozoic and typically have little crustal sulfur with the exception of the Nipissing Gabbro	Common inclusions of country rocks as well as exotic fragments	Massive, inclusion-rich, and disseminated sulfide	Po > Cpy > Pn > Cub	2 (Offset only)	~100 (offset only)	6.2	29	Farrow and Lightfoot (2000)
Tholeiitic	Felsic orthogneiss; no sulfides	Marginal breccia zone	Disseminated	Po > Cpy > Pn > Cub	0.75	~10	6	2.7	Seat et al. (2007)
High-Mg basaltic B1 magma	Dolomites and shales with limited crustal sulfur	None reported	Mostly disseminated	Po > Cpy + Pn	0.4	~10	4	1	Li et al. (2002) and Maier et al. (2004)
High-MgO basalt	Proterozoic sedimentary rocks of Barrager Basin with minor sulfide	None described	Massive and disseminated	Po > Cpy > Pn	0.3	~5	6.5	1.5	Ding (2010)
Picritic basalt	Virginia and Thompson formations with crustal sulfur	Not known	Ragged disseminated with local massive veins	Po > Cpy > Pn	4	~50	n/a	n/a	(Goldner, 2011)
Tholeiite	Gunflint iron formation and Rove shale — locally sulfidic	Pegmatoidal rocks, but not breccias	Reef style disseminated sulfide	Po > Pn > Cpy	18 (excluding Pine River dyke)	~1000	4.2	23	(Naldrett, 2004; Cogulu, 1990; Heaman et al., 2007)
Basaltic magma	Quetico metasedimentary rocks and grabitoids	Hybridized margins	Disseminated and net-textured with local massive patches	Po > Cpy > Pn> > Py	0.3	~5 (in the tubular body)	3.3 (massive)	100	(Goodgame et al., 2010; Smyk and Hollings, 2009)
High-Mg	Schists, gneisses, quartzites, and marbles with disseminated sulfide	Not known	Massive and disseminated	Po > Pn > Cpy	0.25	~20	3	0.25	Glotov et al. (2001)
Tholeiitic	Vorontsov sandstone and shale	None described	Massive and disseminated	Po > Pn > Cpy	1 (Elka), and 1 (Elka)	~10	12-16 (Elan) and 2–4 (Elka)	1.5	(Chernyshov, 2004)
High-Mg	No	Massive sulfide is associated with fragments (durchbewegung)	Massive, net-textured, and disseminated	Po > Pn > Cpy	0.2	~5	9	n/a	(Mungall et al., 2010)
Tholeiitic	Tickalara metamorphic suite: Migmatitic paragneiss with sulfide	Inclusions of paragneiss in mineralised sequence	Disseminated and massive	Po > Cpy > Pn	4	~100	n/a	n/a	(Page and Hoatson, 2000; Thornett, 1981)

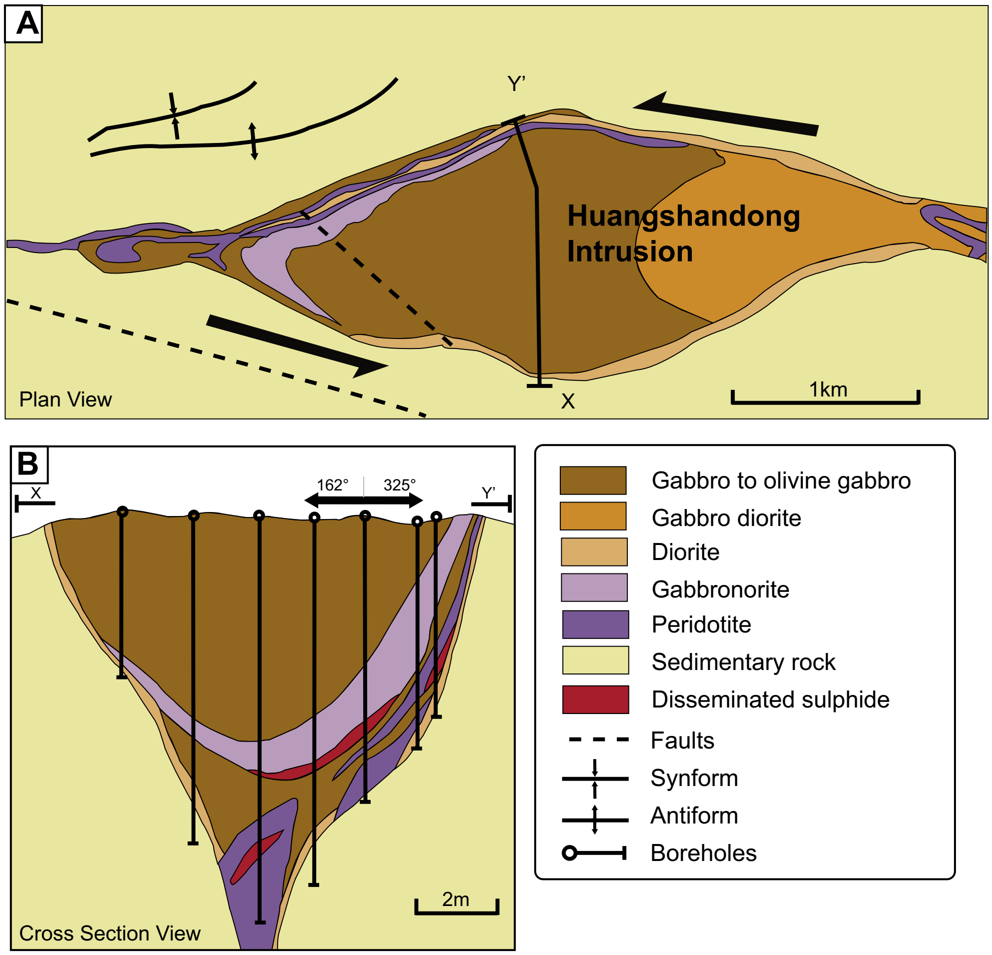

Fig. 3. A. Geological plan of the Huangshandong Intrusion (after Wang et al., 1987); B. West-facing geological cross section through the Huangshandong Intrusion (after Gao and Zhou, 2012; Wang et al., 1987).

Fig. 5A–D and reported by Tang (1993) are consistent with emplacement of the magma and the entrained sulfides into a sub-vertical structure which was possibly a cross-linking structure within a strike-slip segment of the Longshoushan fault zone.

2.3. The Kalatongke Deposit, Fuyun Fault Zone, northern Xinjiang

The Kalatongke Intrusion is located in northern Xinjiang within the broad boundary of the Fuyun fault zone (Fig. 2A). The intrusion is a 305 +/− 15 Ma old (Han et al., 2006) differentiated gabbroic body comprising disseminated and massive nickel sulfides that comprise the third largest mined resource of massive sulfide in China (Fig. 1). The intrusion outcrops at surface in an area of approximately 750 m^2 as a zoned body with a core of olivine biotite hornblende norite and a margin of biotite diorite (Fig. 6A–B; Gao et al., 2012; Wang et al., 1992). The long axis of the intrusion at the surface is aligned sub-parallel to the Fuyun fault zone, and at depth the plunge of the intrusion flattens and the cross-section shape of the intrusion is an ovoid channel that extends to the SE, cutting from west to east across a series of folded Carboniferous-aged sedimentary rocks. The intrusion is thickest in the synformal zones of the country rocks, and appears to narrow as it passes through the anticline in the country rocks. The broad geometry of the intrusion is shown in long section in Fig. 6B and a series of NE–SW sections is shown in Fig. 6C. The sense of displacement along the regional extension of the Fuyun Fault zone is a dextral strike-slip motion (Cunningham and Mann, 2007) and a right-stepping jog and cross-linking structures created a localized transtensional space to produce the rhomboid-shaped outcrop pattern of the intrusion (Fig. 6A).

2.4. The Jingbulake Deposit, Nalataishan Fault Zone, western Xinjiang

The 454 Ma Jingbulake Intrusion (Yang et al., 2012) is located in the western Tian Shan Belt (Fig. 2) within the Nalatishan Fault Zone. The intrusion is about 4 km long by 1.5 km wide, with the long axis of the intrusion elongated sub-parallel to the Nalatishan Fault Zone. The intrusion is a concentrically zoned body comprised of olivine gabbro and wehrlite core surrounded by a thick interval of olivine gabbro which is separated from country rock gneisses by pyroxenite, hornblende gabbro and diorite (Fig. 7; Yang et al., 2012). The sulfides that crop out close to the surface are typically disseminated in olivine gabbro and comprised of pyrrhotite, pentlandite and chalcopyrite. The marginal rock type of the intrusion is dioritic in composition, and locally shows a fabric parallel to the contact of the intrusion. Geological relationships between country rocks and the intrusion are both magmatic contacts and structures, and the deep structure remains uncertain, however the similarity to the zonation of Huangshandong indicates that the intrusion may have a funnel-shaped keel and stem-like feeder dyke at depth. The sense of displacement of the Nalatishan fault zone is less clear as there has been N–S shortening, but it is believed to be sinistral, and forms the western extension of the Kangguer Fault which is left lateral in displacement (Mann, 2007). The broad geometry of the intrusion which is elongated ENE–WSW with the northern and southern contacts sub-parallel to the fault zone, is consistent with the development of space in a cross-linking structure at a left-stepping fault with sinistral displacement.

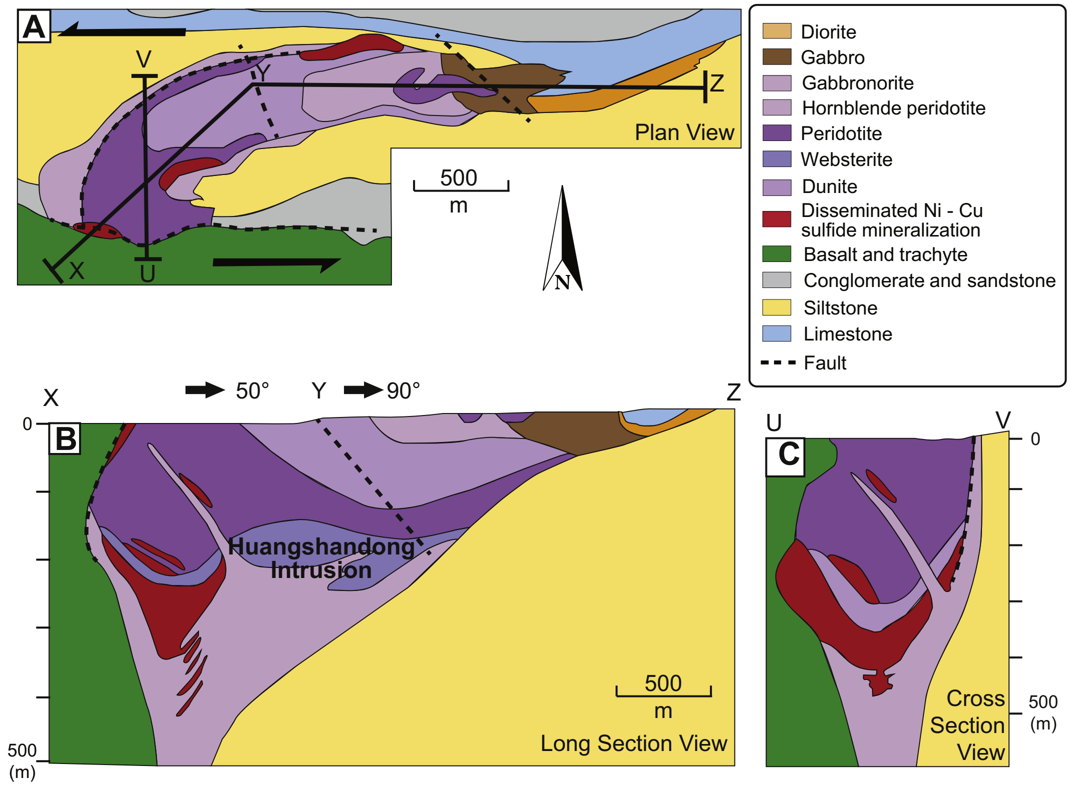

Fig. 4. A. Geological plan of the Huangshan Intrusion (Wang et al., 1987); B. NW and N-facing long section through the Huangshan Intrusion (Wang et al., 1987). C. West-facing cross section through the Huangshan Intrusion (Wang et al., 1987).

2.5. The Hongqiling Deposits, Huifeihe structural zone, Jilin Province

The Ni deposits in Jilin Province, NE China, are part of an ~217 Ma intrusive event within the stratigraphy of the Hulan Group (Lü et al., 2011; Wei et al., 2013; Wu et al., 2004). The intrusions are typically small (<0.5 km^2 in surface area) and differentiated with the more ultramafic rock types containing the mineralization (Table 1). Fig. 8A shows the geology of the Hongqiling region where a series of NW–SE structures contain small intrusive rock bodies with their long axes oriented sub-parallel to the fault zone; these faults join up with the Huifeihe graben to the south and are possibly subsidiary faults of the main ENE–WSW structure. The sulfide mineralization varies from disseminated to massive sulfide, with the Hongqiling Number 1 and Number 7 intrusions being the richest historic producers in the belt.

The Number 1 intrusion is mineralized with disseminated sulfide that is typically interstitial grading into comingled blebs; the sulfides have similar Ni-tenors to the massive sulfides. The Number 1 intrusion has an original shape of an elongate lens with faulted contacts on the western side and uncertain geological relationships with the gneisses on the eastern side; the intrusion was about 700 m long and 300 m at the widest point prior to mining, with an internal stratigraphy comprising mineralized olivine pyroxenite at the margin, through pyroxenite to gabbro at the core (Fig. 8B–C). The morphology of the Number 1 intrusions is broadly similar to Huangshandong and Jingbulake; it is speculated that the primary morphology of the intrusion is controlled by a cross-linking structures within a jog between two strike-slip faults.

The Number 7 intrusion has the form of a dyke comprised largely of pyrrhotite–pentlandite +/-pyrite-bearing orthopyroxenite with a very high ratio of sulfide relative to silicate magma and a high Ni tenor (14–15% Ni in 100% sulfide; Wei et al., 2013); the intrusion sits within a structure which has been reactivated after deposition of Cenozoic conglomerates such that the SE wall of the pit is now a graben structure, possibly reactivated at the time of development of the NNE–SSW trending Huifeihe Graben at the northern margin of the Sino-Korean Shield (Fig. 8A). The orthopyroxenites at the core of the dyke are typically fresh, but the margins of the intrusion typically show deformation.

2.6. The deposits associated with the Emeishan Large Igneous Province, Yunnan and Sichuan Provinces

A number of weakly to heavily mineralized intrusions are associated with small differentiated intrusions in the roots of the 260 Ma Emeishan large igneous province in Yunnan and Sichuan Provinces of SW China (the area shown is underlain by numerous small intrusions; Fig. 9A). Many of the intrusions are located in association with north–south trending fault structures which have previously been referred to as the "Panxi Rift" (Zhang et al., 1988) and are more likely deep-seated structures in the basement which have been reactivated and controlled some of the migration paths of magma from mantle to surface; collectively we term these structures the Panxi faults. Many of these faults are poorly understood due to the deep weathering profile, but at least some local parts of the fault system show dextral strike-slip displacement along fault segments.

A number of examples of medium-sized to small deposits are developed in association with intrusions injected along minor N–S faults; these include Yangliuping (Song et al., 2003) and Baimazhai (Tang, 1993).

The differentiated Limahe Intrusion (Fig. 9B–C) comprises a body which is ~2 km^2 in plan view, yet hosted a medium-sized Ni–Cu deposit (Fig. 1). The intrusion is comprised of olivine pyroxenite, peridotite, gabbro and diorite within quartzites and shales of the Huili Group. The intrusion is an elongate rhomboid-shaped body with a narrow keel which joins to a dyke at depth. The intrusion shows an irregular concentric zonation pattern of mafic and ultramafic rock types, but the keel and marginal rocks are typically peridotites and these rocks contain the massive and disseminate sulfide mineralization (Table 1).

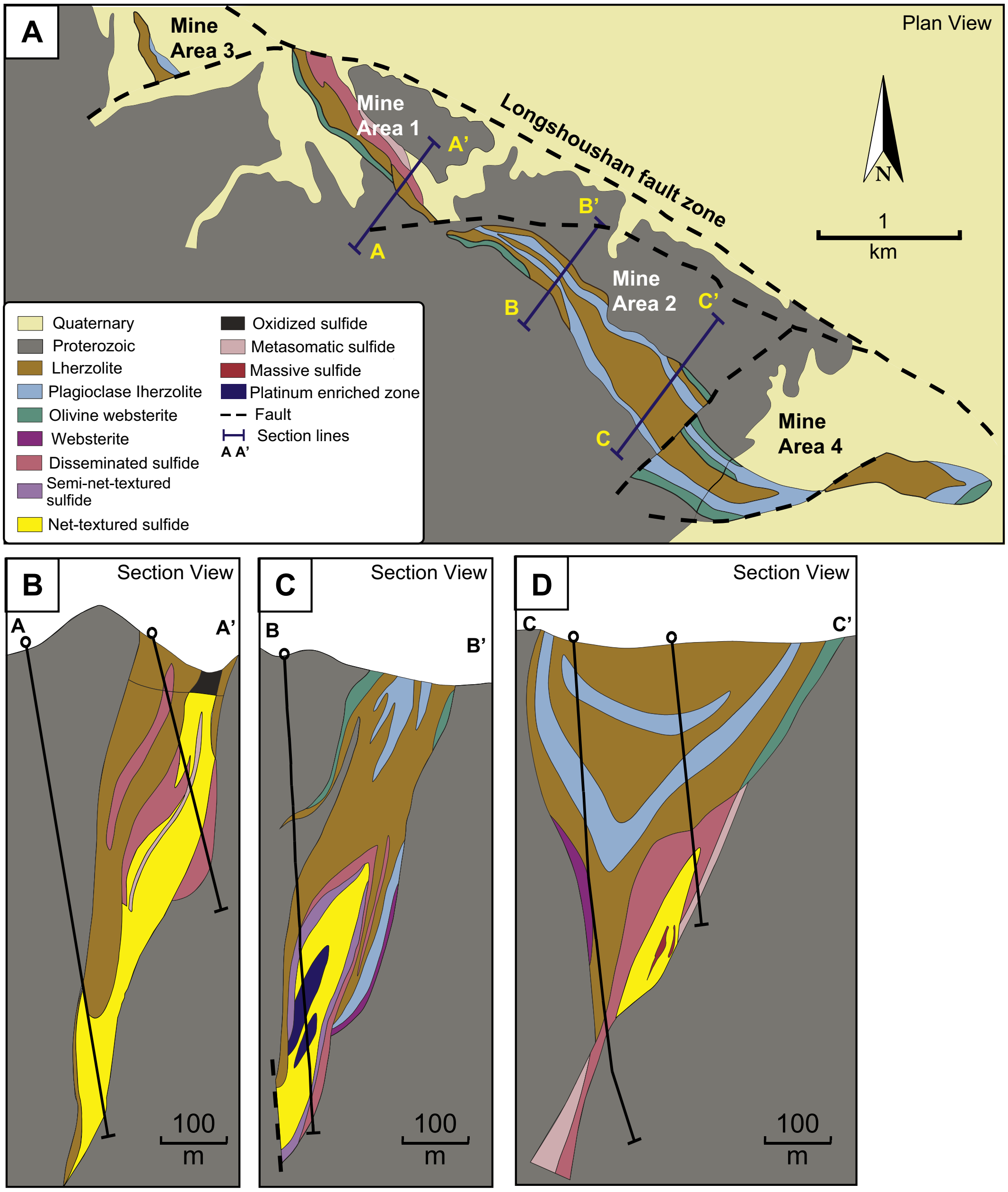

Fig. 5. A. Simplified geological map of the Jinchuan Intrusion showing the location of major faults. B. NW-facing geological cross section through Mine Area Number 1. C. NW-facing cross section through the western part of Mine Area Number 2. D. NW-facing cross section through the SE part of Mine Area Number 2. Diagrams are modified after Tang (1992).

Another small example of a similar fault-controlled intrusion is located in southern Sichuan; Qingquanshan is a small intrusion with a dyke-like keel associated with the intersection of the Anning River (N–S) and Yimen (W–E) fault structures in the Huili Group Hekou Formation limestones (Fig. 9D–E). This intrusion consists of peridotite and gabbro and is elongated in a N–S direction with an original outcrop extent of just 150 × 30 m, and reaching a depth of 170 m for the base of the mineralized peridotite margin as well as the conduit at depth.

The Jinbaoshan intrusion which contains a Pt-enriched disseminated sulfide mineral zone is developed within the Red River Fault at the SW margin of the Emeishan (Fig. 9A; Wang and Zhou, 2006; Wang et al., 2006). This intrusion resides within a sinistral strike-slip fault zone. The Baimazhai Intrusion in Yunnan (Tang, 1992) and the Ban Phuc Intrusion in Vietnam (Glotov et al., 2001) are adjacent to the same major fault zone.

2.7. Summary of common traits of the Ni sulfide deposits of China

A number of features are shared in common by the group of nickel deposits located in China (Table 1). The key traits of the deposits are asummarized as follows.

1. The host intrusions are typically small in volume and outcrop/subcrop area. Jinchuan has a surface outcrop area of ~1.5 km^2 and other intrusions are typically less than 2 km^2.
2. The intrusions are composed of rock types that include dunite, peridotite, wehrlite, lherzolite, pyroxene peridotite and olivine gabbro in association with mineralization, and gabbro, gabbronorite, and diorite in weakly mineralized or unmineralized parts of the intrusions (e.g. Table 1).

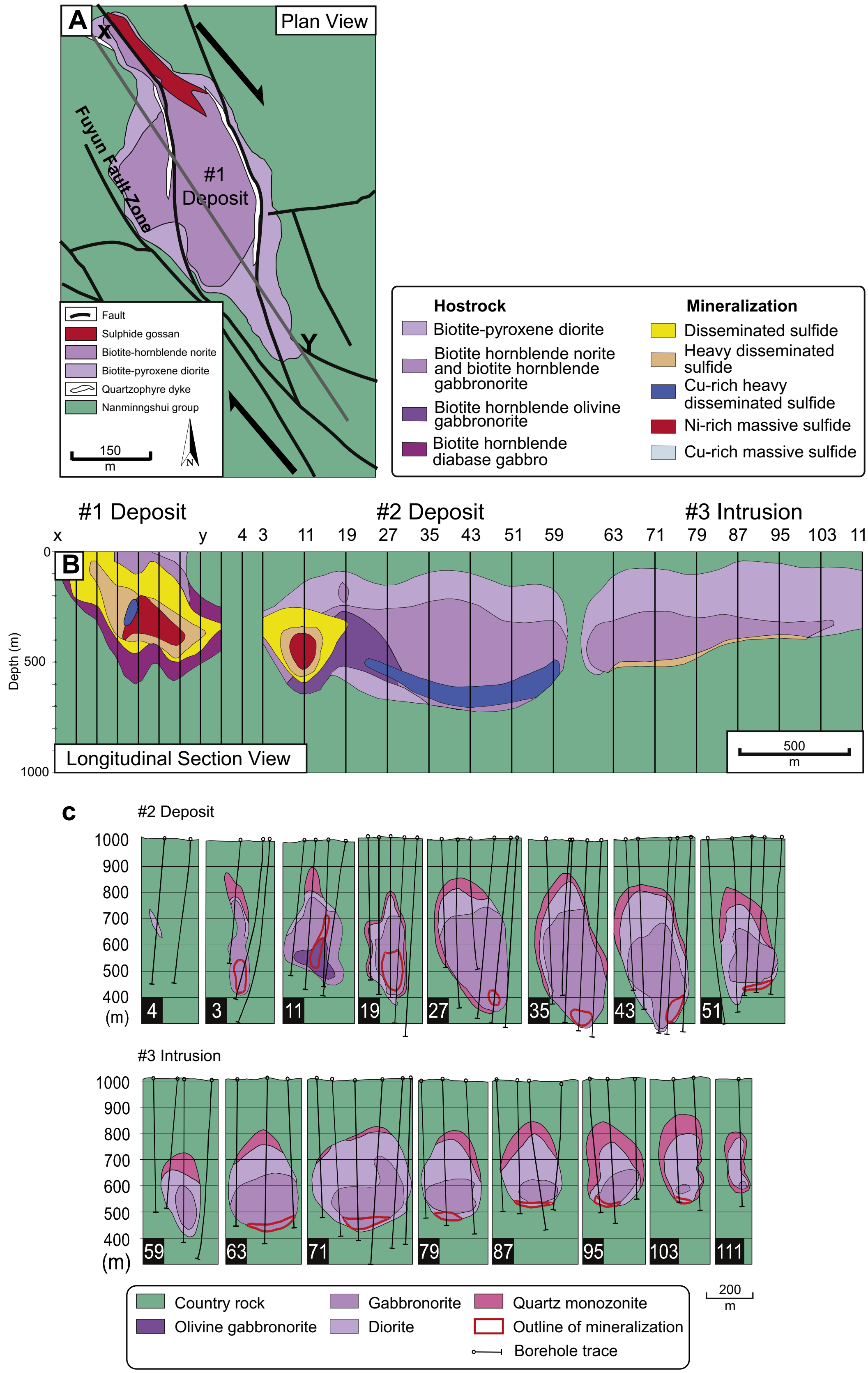

Fig. 6. A. Geological map of the Kalatongke Intrusion. B. Long section through the Kalatongke Intrusion, extended at depth to the SSE, showing the position of the intrusion and the distribution of rock types and mineralization. Note that only the Number 1 intrusion crops out at surface as shown in Fig. 6A. C. A series of cross sections through the Number 2 and Number 3 segments of the intrusion showing the geometry of the contacts and the distribution rock types and mineralization. After Wang et al. (1991, 1992).

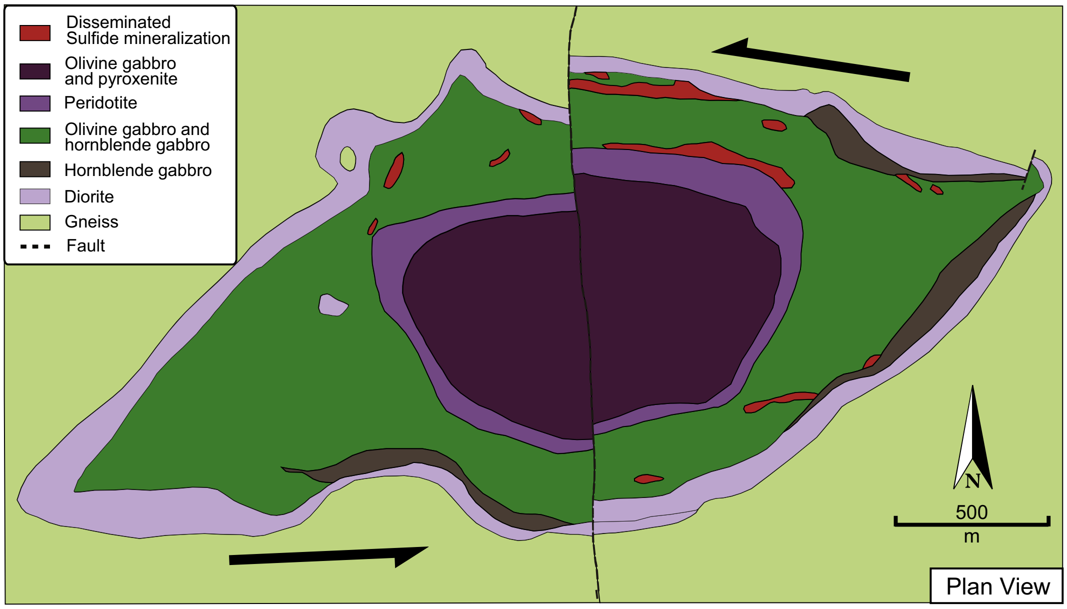

Fig. 7. Geological map of the Jingbulake Intrusion showing the distribution of rock types and Ni–Cu sulfide mineralization. After Yang et al (2012).

3. The Chinese deposits show a spectrum of morphologies including rhomboid-shaped funnels, dyke-like sheets, and oblate channels.
4. Mineralization is normally related to the keel of the intrusion.
5. The volume of sulfide relative to silicate rock is high, and so the metal and S content of the mineralization cannot be generated from the observed volume of silicate magma.
6. The intrusions are within strike-slip transtensional zones and are located at jogs or cross-linking structures where the strike-slip displacement is offset, creating a localized transtensional space into which magma can be emplaced to form the intrusion. These structures are often reactivated during deformation which can explain the diversity in rock types and overprint the contacts and evidence for previous motion.
7. The rhomboid-shaped intrusions are often contiguous with a dyke which connects at the keel of the intrusion. The various intrusions appear to be part of a connecting trellis of intrusions and conduits which form a complex pathway from the mantle to the surface.
8. There is generally little evidence of association of the small intrusions with country rock sulfide, and so the source of the S is generally considered to occur at depth (e.g. Tang, 1992). The elevated sulfide/silicate ratio found within each of the intrusions is indicative of emplacement of sulfide magmas or sulfide-laden magmas (e.g. Lightfoot, 2007; Tang, 1992) rather than in-situ segregation and accumulation of sulfide from the magma contained in the chamber. It appears likely that many of the Chinese magmatic sulfide deposits have S achieved S saturation through assimilation of crustal S at depth (e.g. Gao et al., 2012; Wang et al., 2012; Yang et al., 2012).

3. Geology of the Noril'sk–Talnakh Deposits, Siberia, Russia

The world-class Noril'sk–Talnakh Ni–Cu–PGE sulfide deposits in Russia are associated with intrusions that have been extensively studied by a generation of Russian experts who mapped and logged drill core from the Noril'sk Region (e.g. Kunilov, 1994, and references therein). The Noril'sk Ni–Cu–PGE sulfide deposits are located at the NW margin of the Siberian Shield, and inboard to the east of the margin of the Siberian Craton (Fig. 10A). The Noril'sk Deposits are juxtaposed close to the Noril'sk–Kharaelakh Fault beneath or within the basal flows of the Siberian Trap basalts (Fig. 10B). The geology of the Noril'sk Region is comprised of a sequence of unexposed basement rocks that form the Siberian Craton, overlain by Proterozoic-aged metasedimentary rocks, followed by a sequence of Devonian and Permian shallow marine and sabkha stratigraphy containing intermittent packages of deeper water shales (e.g. the Razvedochninsky Formation) and evaporates throughout the sequence with Carboniferous coal-measures and shales (Fig. 10C). These rocks are overlain by the Siberian Trap flood basalts and tuffs which comprise an almost continuous stratigraphy of nine different formations in the Noril'sk Region (e.g. Lightfoot et al., 1990, 1993). The entire package of sedimentary and volcanic rocks is cut by a complex network of faults, and folded on a regional scale to form basins and arches. The faults comprise a major group of NNE–SSW structures including the Noril'sk–Kharaelakh and Imangda Faults; displacement along the faults varies in magnitude and direction with the strike-slip and a reverse sense of motion (Mezhvilk, 1984; Yakubchuk and Nikishin, 2004) which varies in extent and sense of displacement along the length of the fault (Mezhvilk, 1984, 2004).

The dominant center of accumulation (depocenter) of metal-depleted basaltic rocks of the Nadezhdinsky Formation of the Siberian Trap is localized along the axis of the Noril'sk–Kharaelakh Fault, and this volcanic edifice has a volume of 5000–10,000 km^3 (Fig. 10B), from which up to ~99% of the precious metals and up to ~80% of the Ni, Cu, and Co have been removed as a response to equilibration of the parental magma with magmatic sulfide (Lightfoot and Keays, 2005; Naldrett et al., 1995). This volcanic edifice is underlain by sedimentary rocks which contain intrusions that are more primitive than the basaltic rocks, but have similar ages and trace element ratios which indicate that they belong to a magma series that is temporally and spatially related (Naldrett et al., 1995). These include the strongly differentiated and weakly mineralized Ni–Cu–PGE-depleted Low Noril'sk and Low Talnakh Intrusions which underlie the economically mineralized intrusions at Noril'sk and Talnakh (Figs. 10B, 11). The Talnakh, Kharaelakh, and Noril'sk Intrusions are heavily mineralized and are positioned stratigraphically above the Low Talnakh and Low Noril'sk Intrusions and cross-cut the stratigraphy of the sedimentary rocks beneath the Siberian Trap, and in the case of the Noril'sk 1 intrusion, the most basal Ivakinsky and Syverminsky Formation basalts of the Siberian Trap. The Talnakh and Kharaelakh Intrusions are located adjacent to the Noril'sk–Kharaelakh Fault, but appear not to be fed along the main fault (Figs. 10B, 11). The Talnakh intrusion is at a higher stratigraphic level in Permian sedimentary rocks than the Kharaelakh Intrusion which is hosted in Devonian-aged sedimentary rocks. The main part of the intrusion is within argillites of the Razvedochinsky and Tungusskaya

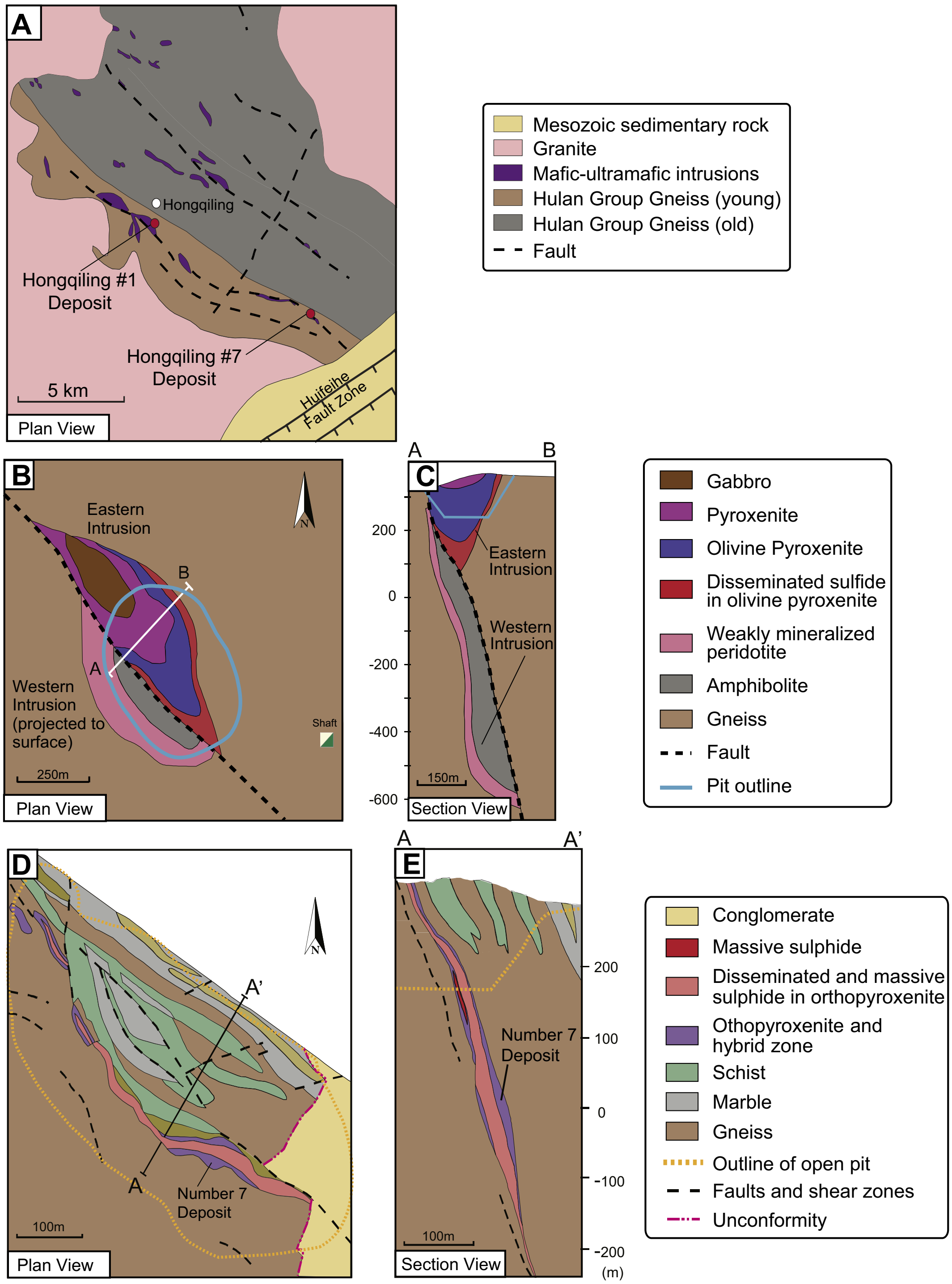

Fig. 8. A. Geology of the Hongqiling area showing the distribution of mafic–ultramafic intrusions associated with structures cutting through the Hulan Group gneisses. B. Geological plan of the Number 1 Intrusion, Hongqiling Belt. C. North-facing geological cross section of the Number 1 Intrusion of the Hongqiling Belt. D. Geological plan of the Number 7 Intrusion and Fujian nickel deposit in the Hongqiling Belt. E. Cross section facing north through the Number 7 Intrusion, Hongqiling Belt. After Wei et al. (2013) and Tang (1992).

series (Fig. 10C), and these sediments are typically missing or partially missing from the sequence along the widest part of the intrusion (Lightfoot and Zotov, 2014; Zotov, 1989).

The shape and form of the Low Talnakh intrusion as described in Zenko and Czamanske (1994) include both weakly differentiated sill-like domains, and thicker heavily differentiated channel-ways as shown in Fig. 12A. The channel-ways are typically localized along segments of the intrusion that are hosted in sedimentary rocks that have a synformal structure, and the thinner sections tend to be associated with antiformal features in the country rocks (Fig. 12A). Although the Low Talnakh Intrusion is Ni-depleted and barren of sulfide mineralization, the rocks show a similar geometry and range of mafic–ultramafic rock types when compared to the economically mineralized Talnakh and Kharaelakh intrusions (e.g. Hawkesworth et al., 1995). The channel-ways in the Low Talnakh Intrusion are distributed both adjacent to the Noril'sk–Kharaelakh Fault and they extend away from the fault where they form a series of wider channels that spatially correspond to the anticlinal structures in the country rocks.

The main conduits of the Kharaelakh Intrusion have a form similar to the Low Talnakh Intrusion as shown in Fig. 12B, but the margins of the

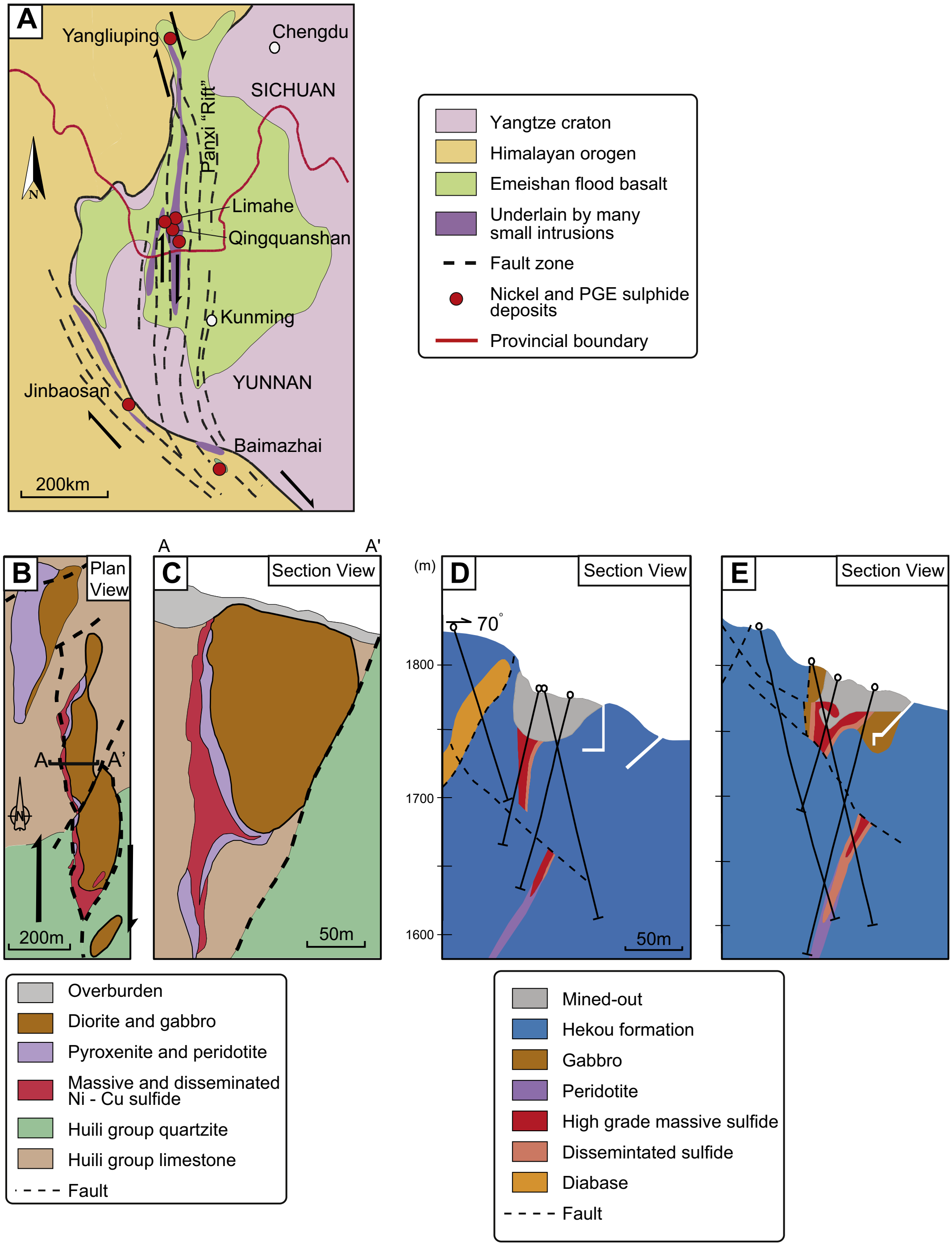

Fig. 9. A Geological map of the Emeishan LIP showing the distribution of flood basalts, major north–south trending structures, domain of sub-volcanic intrusions, and the principal intrusions containing nickel sulfide deposits. After Zhou et al. (2002). B. Geological map of the Limahe Intrusion. C. North-facing cross section through the Limahe Intrusion. D and E. Geological section through the Qingkuangshan Intrusion. After Tang (1993) and Zhu et al. (2011).

sheet comprise flanking domains where the intrusion has complex relationships with the surrounding sediments at a range of scales, viz: 1. Sheet-like apophyses of weakly differentiated sills (termed 'the sills of the Kharaelakh Intrusion' and shown in Fig. 11); 2. apophyses described in Zotov (1989) as 1–10 m thick sills within a wide domain of metamorphosed metasedimentary rocks (also termed "the horns of the Kharaelakh Intrusion"; Zotov, 1989); and 3. local apophyses of gabbroic magma which are chilled where they are in direct contact with the surrounding hornfelsed sedimentary rocks in the form of lobes on the scale of 10–50 cm (termed "the ears of the Kharaelakh Intrusion"; Lightfoot and Zotov, 2007, 2014; Zotov, 1989). The widest parts of the Kharaelakh Intrusion are located where the country rocks have a synformal structure or are rifted parallel to the Noril'sk–Kharaelakh Fault (Fig. 12B). The main zones of basal Ni-rich massive sulfide mineralization are either located at the base of the intrusion or within ~20 m of the intrusion in the underlying sedimentary rocks, and broadly follow the axis of the channels (Fig. 12C after Zenko and Czamanske, 1994). In cross-section view, at the northern end of the Kharaelakh and Talnakh Intrusions, the chambers resemble oval conduits within narrow sheets (Fig. 13A), and the base of these conduits contain the deposits of the Skalisty and Gluboky Mine Areas. The geometry of the Noril'sk I conduits is very similar to the Talnakh and Kharaelakh conduits (e.g. Lightfoot and

Zotov, 2007; Fig. 13B), and although the association is with disseminated sulfides, the same channel-ways control both styles of mineralization.

A feature of both the Talnakh and Kharaelakh Intrusions is the important association of Cu–PGE sulfide mineralization with brecciated country rocks in the footwall exocontact domain of the Talnakh Intrusion, and the hangingwall exocontact domain of the Kharaelakh Intrusion (Fig. 14A). This styles of mineralization typically has elevated Cu and PGE with Cu/Ni ~ 5, but they are low in Ni which contrasts with the differentiated Cu-rich mineralization at the lower contact of the intrusions in the pyrrhotite–pentlandite–chalcopyrite style of Ni-rich ores (Cu/Ni ~ 15) as described in Naldrett et al. (1992, 1995) and Stekhin (1994). In hand sample, these breccias comprise a complex metasomatized assemblage of country rocks with interstitial sulfides between anhydrite crystals (Fig. 14B) and the development of skarn mineralization (Zotov, 1989). The cuprous ores of the lower exocontact at Skalisty Mine area comprise extensively metasomatized country rocks with the Cu mineralization largely controlled by the matrix of the breccia (Fig. 14C).

Tectonic controls on the development of the Noril'sk chonoliths are incompletely understood, but there is clear evidence that local antiformal structures adjacent to the N–K fault have controlled the distribution of the magma channel-ways in the sedimentary rocks. Strike-slip motion on the Kharaelakh Fault is one mechanism by which space can be created for magma channel-ways, and this is also a mechanism that generates local antiformal structures as the sedimentary rocks warp in response to local transpression (e.g. Cunningham and Mann, 2007). The unusual exocontact

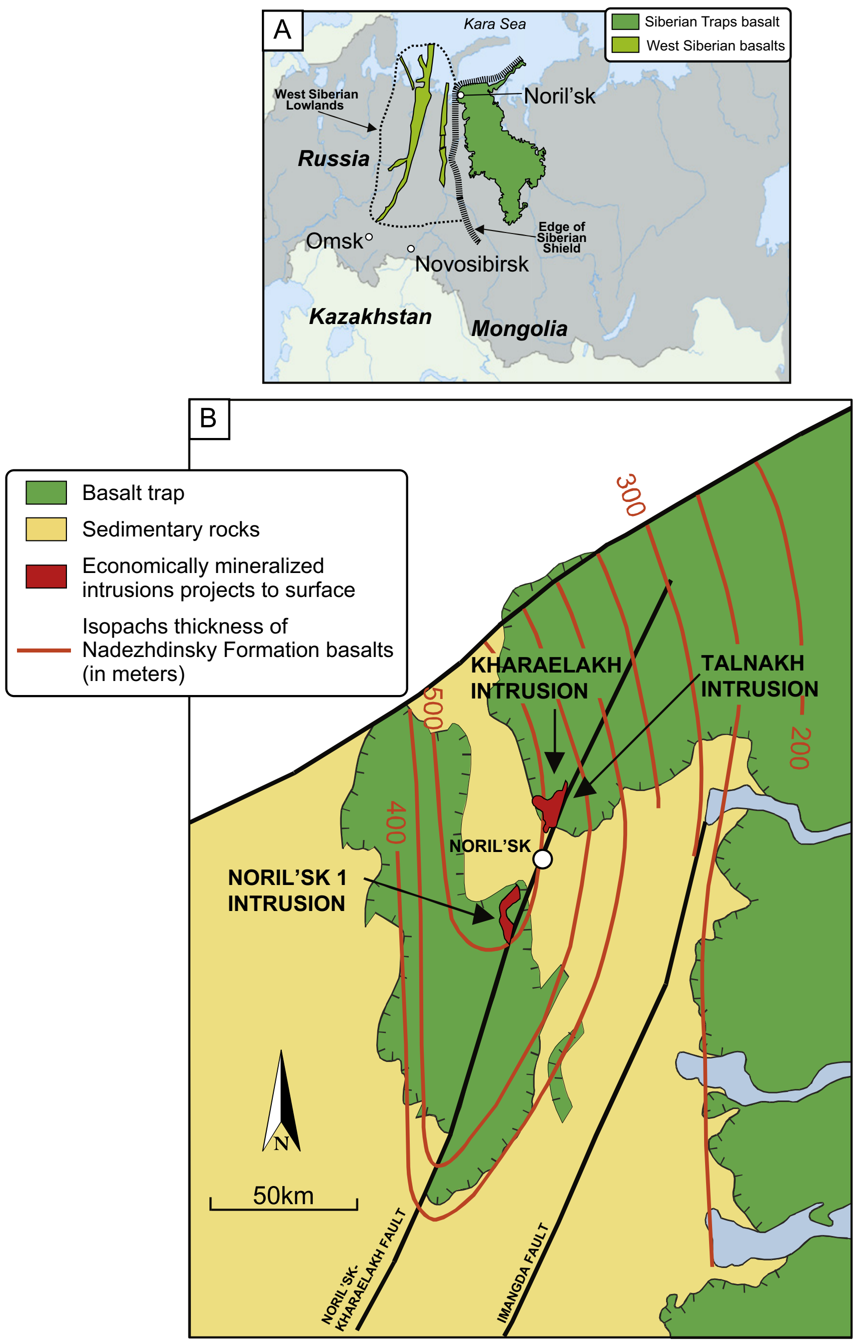

Fig. 10. A. Simplified geology map of the Siberian Trap flood basalts showing the location of the Noril'sk Region, the Siberian Shield, and the West Siberian Lowlands (after Lightfoot and Zotov, 2007). B. Geological map of the Noril'sk Region showing the distribution of basalts and sediments, the principal structures, intrusions, and location of the Ni–Cu–PGE-depleted Nadezhdinsky volcanic edifice (after Naldrett et al., 1995). C. Stratigraphy of the sediments and basalts of the Noril'sk Region (after Zenko and Czamanske, 1994).

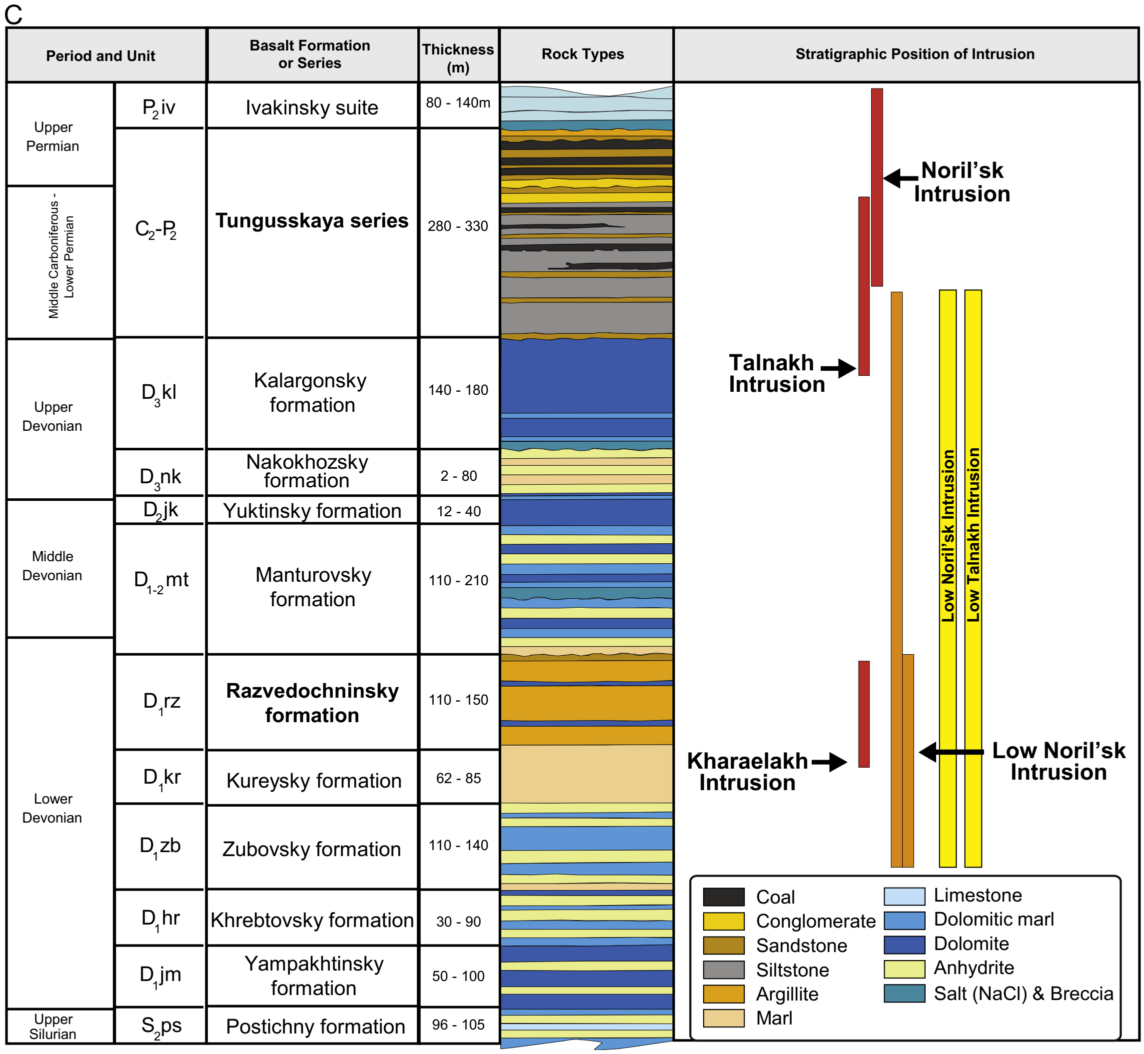

Fig. 10 (*continued*).

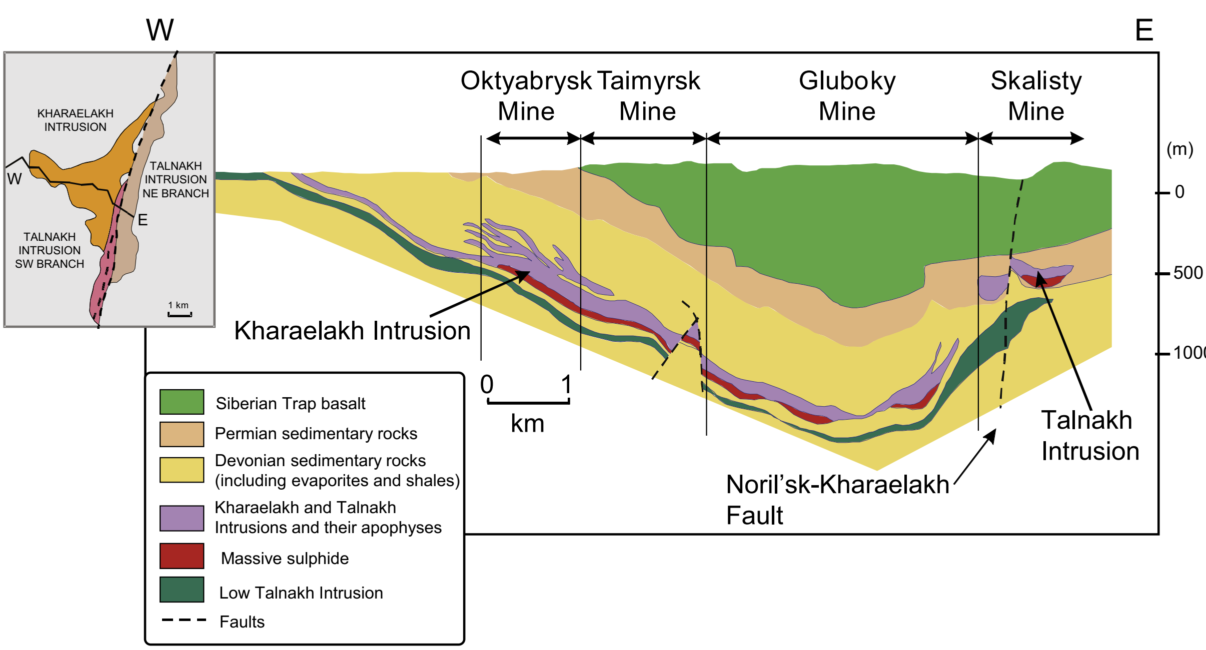

Fig. 11. Geological cross section through the Talnakh and Kharaealakh Intrusions along line shown in inset. After Naldrett et al. (1995).

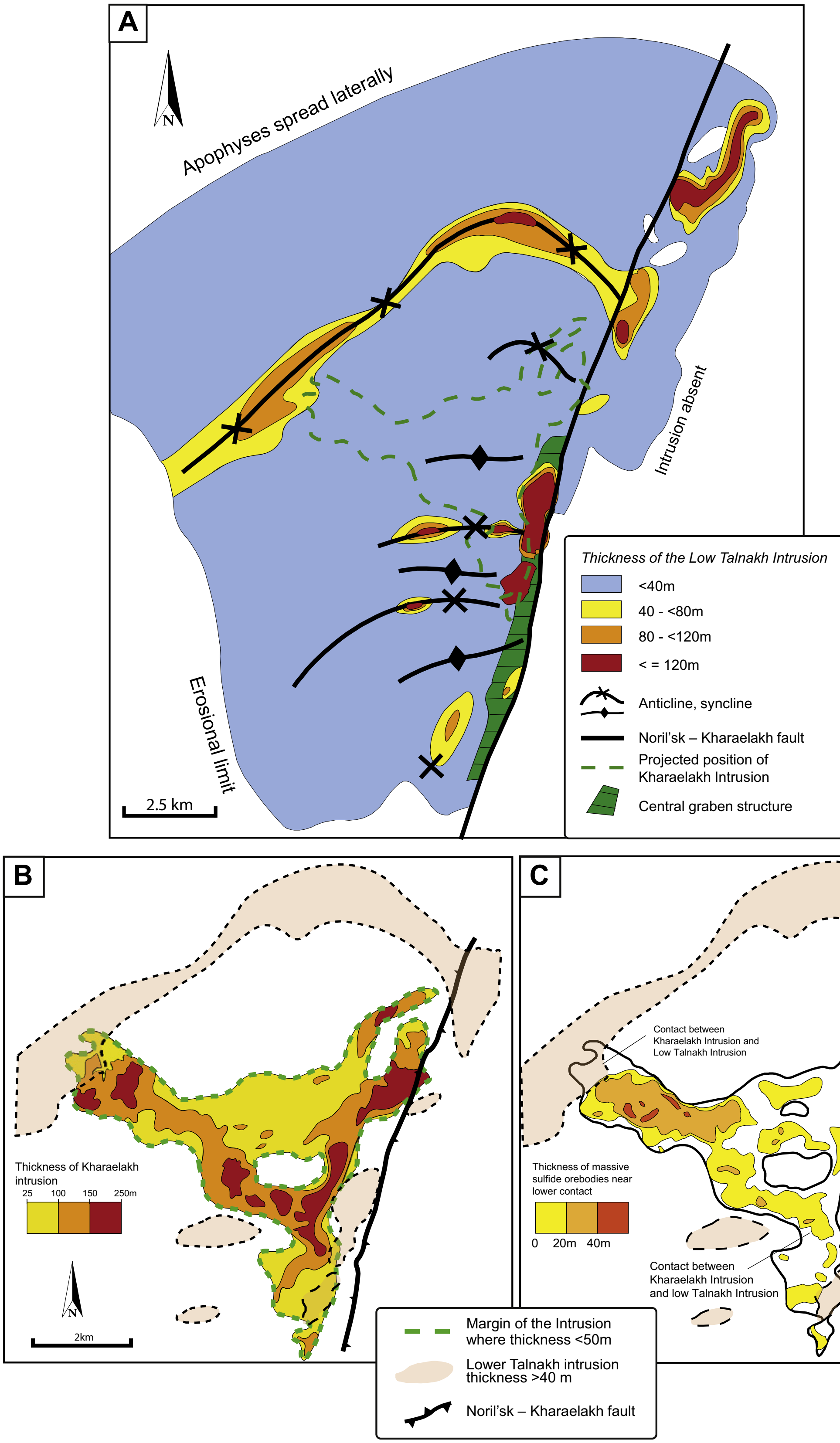

Fig. 12. A. Location and distribution of the Low Talnakh Intrusion, showing the principal differentiated chonolith in relation to structures developed adjacent to the Norilk'sk-Kharaelakh Fault. B. Location and distribution of the Kharaelakh Intrusion, showing the principal differentiated chonolith in relation to structures developed adjacent to the Norilk'sk-Kharaelakh Fault. C. Variations in thickness of massive Ni-rich sulfides at the lower contact of the Kharaelakh Intrusion. After Zenko and Czamanske (1994).

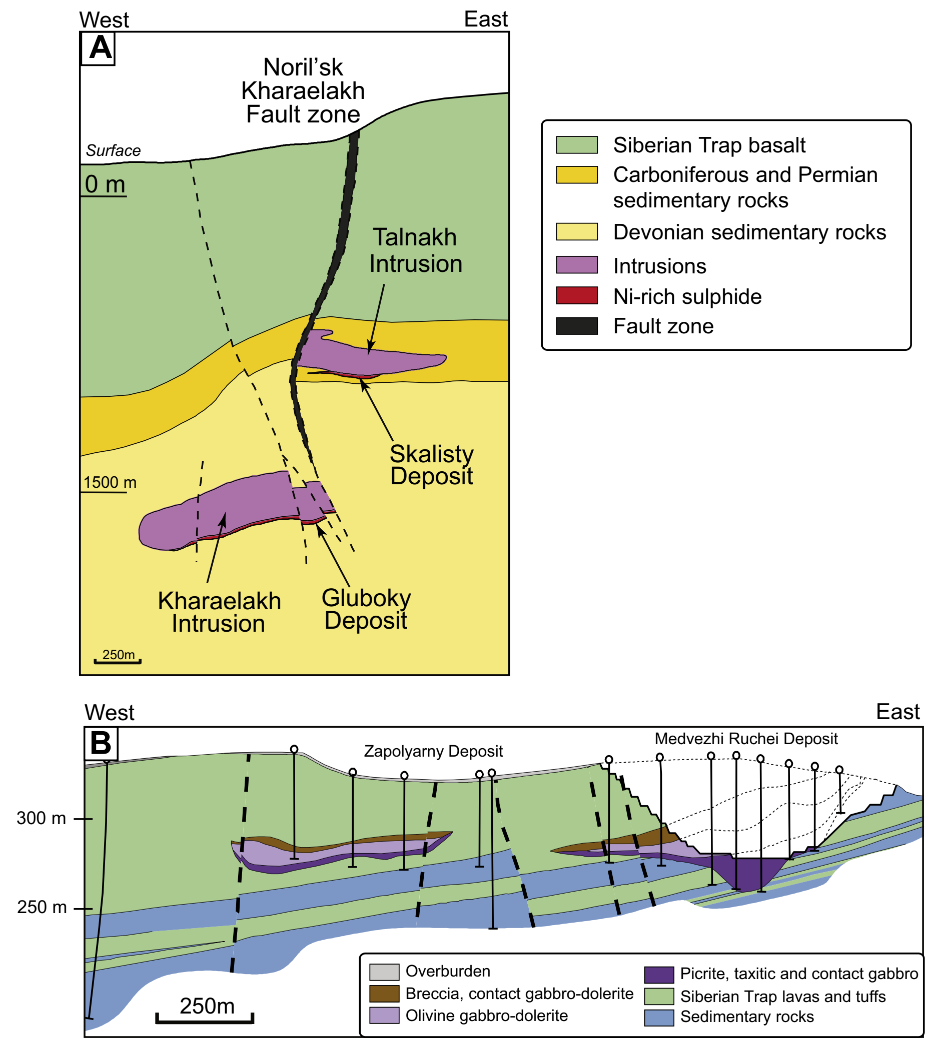

Fig. 13. A. Geological cross section through the Gluboky and Skalisty mine areas at the northern end of the Kharaelakh–Talnakh intrusions. B. Geological cross section through two chonoliths of the Noril'sk 1 Intrusion.

Cu–PGE ores are likely the product of sulfide melt differentiation, but their emplacement is probably controlled by space available within the evolving conduit system. Some of this space was available at the base of the intrusion to the east of the Noril'sk–Kharaelakh Fault, but to the west it appears to have been generated in response to the collapse of roof rocks over the partially crystallized rocks within the chonolith along minor structures parallel to the Noril'sk–Kharaelakh Fault (Lightfoot and Zotov, 2007, 2014).

4 . The Voisey's Bay Deposit, Labrador, Canada

The Voisey's Bay Intrusion is located in Eastern Labrador, Canada along a broad N–S suture between the Churchill Province paragneisses and enderbite orthogneisses to the west and the Archean Nain Gneiss to the east. The deposit was found as an outcome of grass root exploration by prospectors engaged in exploration for diamonds (Naldrett et al., 1996a). An active mine on the Ovoid Deposit with an original reserves of 31.7 Mmt @ 2.83% Ni, 1.68% Cu, and 0.12% Co, is located within a larger mineral system that comprises five significant mineral zones (e.g. Lightfoot et al., 2012a, 2012b). The intrusion is located at the center of a domain of east–west trending structures which form significant topographic features (Fig. 15A). The structures have a sinistral strike-slip displacement, and the same family of west to east-trending faults extends to Greenland. Their latest motion is controlled by extension in the Labrador Sea (e.g. Myers et al., 2008); these are probably reactivated structures as they are localized within a W–E corridor ~50 km either side of Nain and do not extend in such large numbers to the north and south of this corridor (Fig. 15A). Intrusive activity associated with this W–E fault family includes the dykes and intrusions in the Gardar area of SW Greenland, which comprise the 1.35 Ga Gardar Intrusive suite (Upton and Blundell, 1978), and the intrusions of the 1.35–1.29 Ga Nain Plutonic Suit in Labrador (Ryan, 1998, 2000).

4.1. Geometry and structure of the VBI

The 1.34 Ga Voisey's Bay Intrusion crops out in an east–west orientation to the north of Voisey's Bay (Fig. 15A). The intrusion cross-cuts through a series of N–S trending basement gneisses comprising from west to east paragneisses of the Churchill Province, enderbitic orthogneisses of the Churchill Province, and quartzofeldspathic gneisses of the Nain Province. Much of the Voisey's Bay Intrusion is hosted in paragneiss and enderbitic orthogneiss. The intrusion crops out at the surface in the east (the Eastern Deeps Intrusion) and is connected via a dyke-like conduit to a sub-surface chamber in the west (termed the Western Deeps Intrusion). This is shown in Fig. 15B–C in plan (where the mineral zones are shown projected to surface) and a long-section view (projected onto the dyke and the north walls of the intrusions). The Eastern Deeps Intrusion is a tabular body of olivine gabbro, troctolite, and ferrogabbro containing variably assimilated blocks of orthogneiss as well as magmatic breccias laden with paragneiss

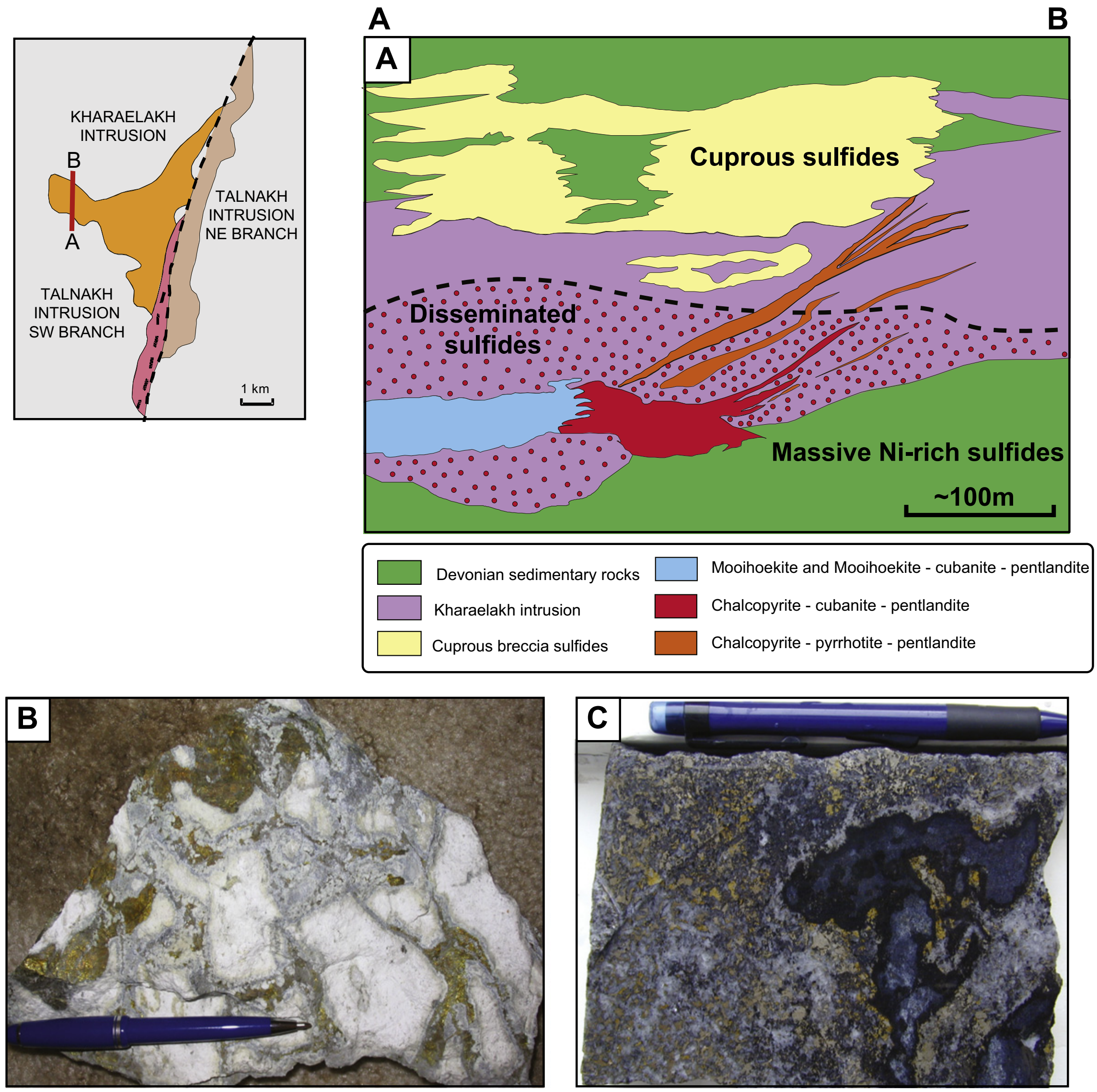

Fig. 14. A. Section showing the geological relationships between the massive Ni-rich ores and the upper exocontact Cuprous ores in the Kharaelakh Intrusion (after Lightfoot and Zotov, 2007). B. Cuprous mineralization developed in metasomatized and brecciated country rocks at the lower exocontact of the Talnakh Intrusion in Skalisty Mine. C. Partially assimilated metasediment clast in marls and evaporates of the upper exocontact of Oktyabrysk Mine.

fragments and magmatic Ni–Cu–Co sulfide mineralization (Lightfoot et al., 2012a, 2012b; Naldrett and Li, 2007). The Eastern Deeps Deposit is located at the base of the northern sub-vertical wall of the intrusion and plunges ~15° ESE along the locus of the entry point of the dyke into the intrusion; this is shown in Fig. 15D in a west-facing cross section through the Eastern Deeps Intrusion and Deposit. The Eastern Deeps Deposit zone is surrounded by a halo of variable-textured troctolite (up to 700 m thick, and extending up to 500 m south of the Deposit within the lower part of the intrusion). The variable-textured troctolite has a range in plagioclase and olivine grain size, with pegmatoidal patches rich in orthopyroxene and ilmenite, and contains 0–20% disseminated magmatic-textured sulfide. The variable-textured troctolite also contains local inclusions of paragneiss (1–10 cm in size) and large pendants of orthogneiss (up to 200 m across), with local hybridized margins. The dyke to the north contains ferrogabbro, olivine gabbro, troctolite, and variable troctolite; a small zone of sulfide mineralization is developed to the north of the Eastern Deeps within the dyke, and this mineralization is termed the "North of Eastern Deeps" (NED) zone (Fig. 15D).

4.2. The Eastern Deeps Intrusion

The shape of the contact of the Eastern Deeps Intrusion is shown in the 3D model reconstructed based on surface mapping and drill core data (Fig. 16). The southern margin of the chamber is poorly understood, largely because it is heavily cut by granitoid rocks at surface, and has limited drilling. The Red Dog Fault marks the southern margin of the Eastern Deeps Intrusion; the fault has a sinistral offset of ~1700 m, and effectively displaces the continuity of the intrusion by 1700 m on the south side of the fault where the Red Dog Intrusion is present. Both the Eastern Deeps and Red Dog Intrusions appear to be part of one original chamber, and the mineral occurrence at Ryan's Pond is consistent with an ESE continuation of the trend of the Eastern Deeps Deposit to the south of the Red Dog Fault, but displaced ~1700 m the East. The gneisses along the north wall of the Eastern Deeps Intrusion have a strong W–E ductile deformation fabric, although there is no clear evidence of displacement along this structure after emplacement of the Eastern Deeps Intrusion. It is possible that this structure was exploited during the development of the magma chamber.

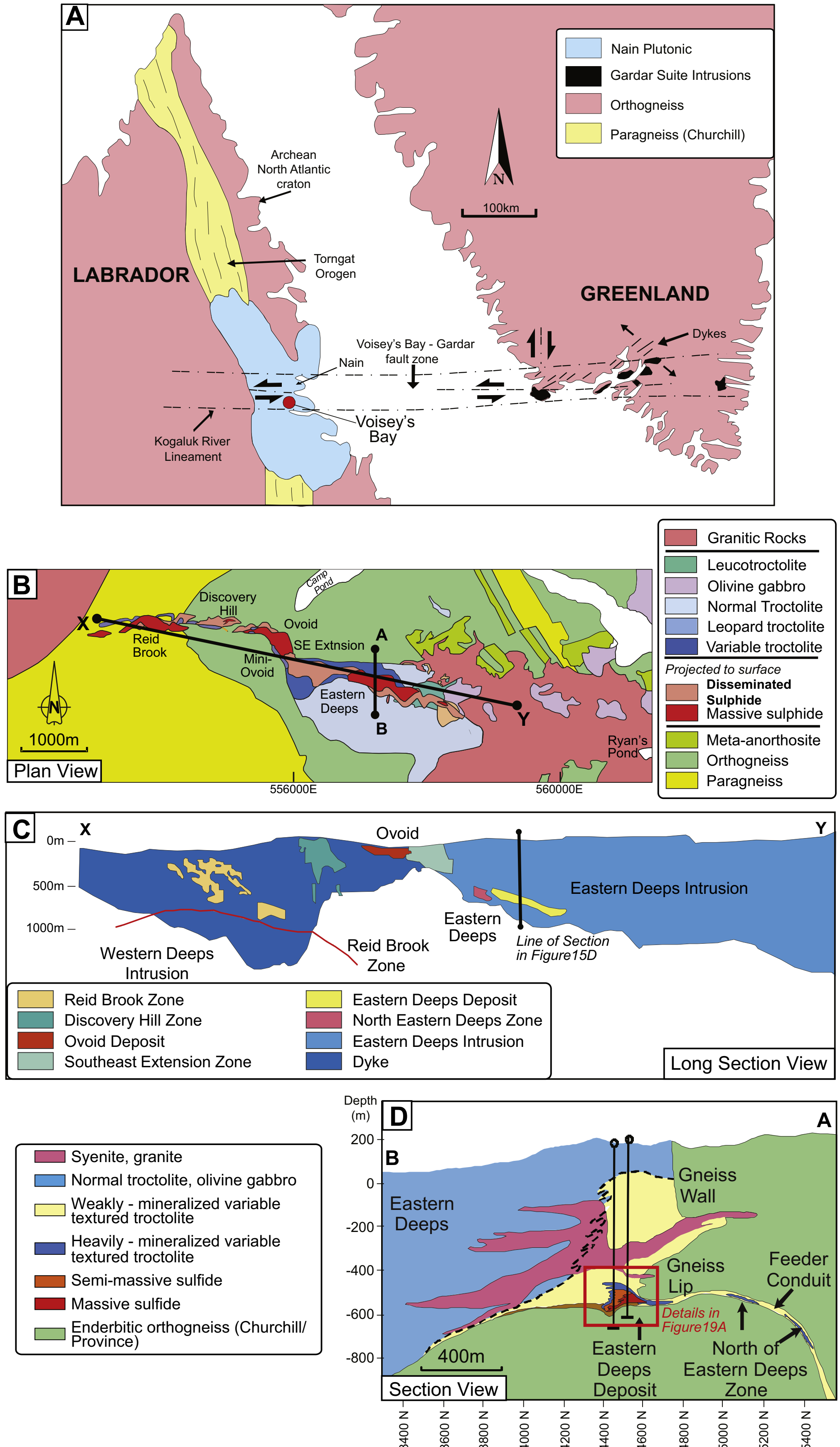
A
Nain Plutonic
Gardar Suite Intrusions
Orthogneiss
Paragneiss (Churchill)
N
100km
Archean
North Atlantic
craton
Torngat
Orogen
LABRADOR
GREENLAND
Dykes
Voisey's Bay - Gardar
fault zone
Nain
Voisey's
Bay
Kogaluk River
Lineament
B
Granitic Rocks
Leucotroctolite
Olivine gabbro
Normal Troctolite
Leopard troctolite
Variable troctolite
Projected to surface
Disseminated
Sulphide
Massive sulphide
Meta-anorthosite
Orthogneiss
Paragneiss
Camp
Pond
Discovery
Hill
X
Reid
Brook
Ovoid
SE Extnsion
A
Mini-
Ovoid
Eastern
Deeps
B
Y
Ryan's
Pond
N
1000m
Plan View
556000E
560000E
C
0m
500m
1000m
X
Ovoid
Y
Eastern Deeps Intrusion
Eastern
Deeps
Line of Section
in Figure15D
Western Deeps
Intrusion
Reid Brook
Zone
Reid Brook Zone
Discovery Hill Zone
Ovoid Deposit
Southeast Extension Zone
Eastern Deeps Deposit
North Eastern Deeps Zone
Eastern Deeps Intrusion
Dyke
Long Section View
Depth
(m)
D
A
B
200
0
-200
-400
-600
-800
Syenite, granite
Normal troctolite, olivine gabbro
Weakly - mineralized variable
textured troctolite
Heavily - mineralized variable
textured troctolite
Semi-massive sulfide
Massive sulfide
Enderbitic orthogneiss (Churchill/
Province)
Eastern
Deeps
Gneiss
Wall
Gneiss
Lip
Feeder
Conduit
Details in
Figure19A
Eastern
Deeps
Deposit
North of
Eastern Deeps
Zone
400m
Section View
3400 N
3600 N
3800 N
4000 N
4200 N
4400 N
4600 N
4800 N
5000 N
5200 N
5400 N

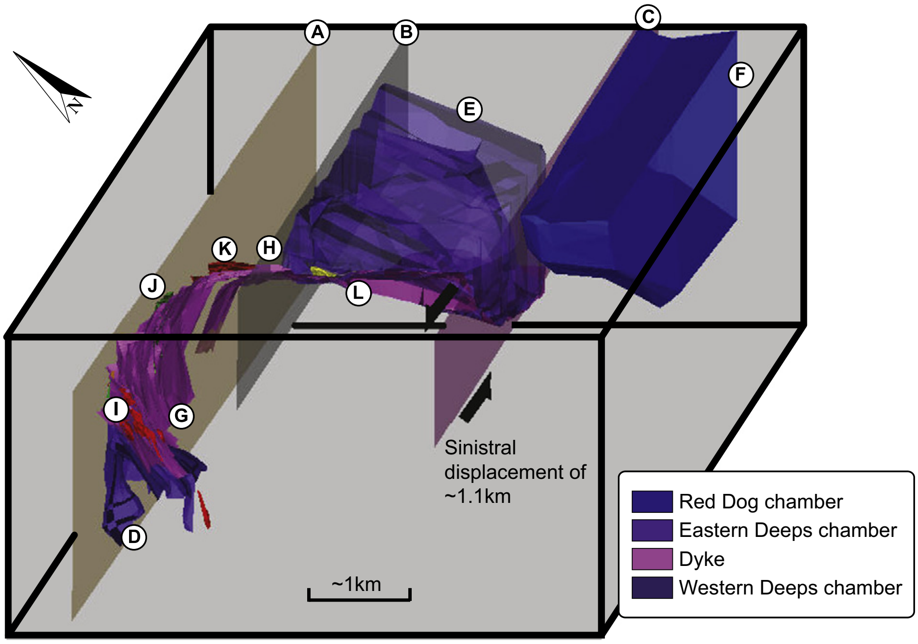

Fig. 16. 3D structural model for the Voisey's Bay Intrusion based on surface geological maps and drill core observations. A — Plane of axis of conduit dyke which appears to be a pre-emplacement fault zone; B — Boundary structure representing the North Wall of the Eastern Deeps Intrusion; C — Red Dog fault; sinistral strike-slip fault with 1100 m displacement; D — Western Deeps Intrusion; E — Eastern Deeps Intrusion; F — Red Dog Intrusion (the south part of the Eastern Deeps Intrusion); G — Ovoid conduit dyke; H — Horizontal splay of conduit feeding Ovoid; I — Reid Brook Zone plunges eastward along the dyke at ~45°; J — Discovery Hill mineral zone; K — Ovoid and Mini-Ovoid deposit; L — Eastern Deeps Deposit.

4.3. Geological relationships and internal structure of the Eastern Deeps

The Eastern Deeps Intrusion comprises a series of unmineralized cumulate-textured weakly layered olivine gabbros and troctolites (Fig. 15D). Some of the troctolites develop stellate clusters of plagioclase feldspar and strong lamination of plagioclase in rocks which are typically devoid of sulfide. Despite the textural variety in plagioclase, they are locally termed "normal-textured troctolites". Within these troctolites are discontinuous units of melatroctolite on the scale of 1–15 m in thickness (Fig. 17A) that dip 20° to the south. Above the normal-texture troctolites is a package of olivine gabbros and gabbros which form an unsubdivided unit that extends towards the eastern margin of the intrusion and south to the Red Dog Fault in areas with extensive development of the Voisey's Bay granite (Fig. 15B). The mineralized troctolites comprise a series of rocks that are termed variable-textured troctolites (VTT) that extend along a west–east trend adjacent to the north wall of the intrusion (Fig. 15D).

Detailed drilling of the Eastern Deeps Intrusion indicates the presence of at least one major pendant (~100 m vertical extent and about 250 m lateral extent) of banded quartzofeldspathic orthogneiss to the south of the Eastern Deeps Deposit which defines the southern boundary of the variable-textured troctolite (Fig. 15D). The margins of these gneiss fragments have complex relationships with the variable troctolite; there is often local evidence of heavy assimilation in the form of partially assimilated gneiss within a matrix of heavily contaminated troctolite through to segregations of partial melts of orthogneiss and relict fragments within the troctolite (Fig. 17B). The blocks appear to be derived from the chamber walls, and it appears likely that they are the remains of the country rocks that were broken up in fault zones or spalled-off the chamber walls during early development of the magma chamber and subsequently surround by the mafic magma which reacted with the blocks to produce the hybridized rocks and variable-textured troctolites.

The inclusion-laden olivine gabbro and troctolite that occur in association with sulfide mineralization (Fig. 19A) have a fabric defined by the elongation of 5–75% paragneiss inclusions (aspect ratios of 10:1 to 100:1 and units of "condensed breccia" which comprise aligned stacked fragments of paragneiss with minimal trapped magma between the fragments (Evans-Lamswood, 2000; Evans-Lamswood et al., 2000), trains of mica and sulfide in the matrix, and the development of ductile structure parallel to the long axes of the inclusions (Fig. 17C). Sometimes relict quartzofeldspathic gneiss lenses remain within weakly mineralized variable troctolite (Fig. 17D). The alignment of fabrics in the breccia sequences of the dykes is generally parallel or sub-parallel to the steep contact, whereas those associated with the Ovoid and Eastern Deeps Deposits tend to follow the flatter geometry of the contact. Within the Eastern Deeps Intrusion, Lightfoot et al. (2012a, 2012b) show that the interface between low and high Ni tenor sulfide occurs along these internal chamber structures (Fig. 19A). The development of the flat ductile structures controls the shape of the mineralization within both the chamber-hosted and dyke-hosted zones. The massive sulfides, breccia sulfide and leopard-textured sulfides comprise the main economic core of the Eastern Deeps Deposit as shown in Fig. 19A, C–D.

The Eastern Deeps Intrusion is cut by late tabular sheets of granite which locally form complex breccias with troctolite and olivine gabbro fragments in a granitic matrix. The sheets of granite range from cm-scale to 150 m in thickness and although continuous between some drill holes, they break-up and re-join laterally such that the distribution of the granite domain is regular, yet the internal geometry is complex. The granitoid rocks do not cut through the deposit or influence the continuity of mineralization. They are largely contained within the footprint of the Eastern Deeps Intrusion, and the intrusions have clearly

Fig. 15. A. Location of the Nain Plutonic Suite (Labrador, Canada), and the Gardar Intrusions in West Greenland (after Myers et al., 2008). A sinistral strike-slip corridor has produced offsets in geology and geomorphology that reflect the opening of the Labrador Sea, but these are likely long-lived structures which controlled the principal orientation of the Voisey's Bay Intrusion. B. Plan view of the Voisey's Bay Intrusion in the immediate area of the deposit (after Lightfoot et al., 2012a, 2012b). C. Long section showing the location of the principal mineral zones in relation to a west–east dyke which connects the Eastern Deeps chamber to the Western Deeps chamber (after Lightfoot et al., 2012a, 2012b). D. West-facing cross section showing geological relationships in the Eastern Deeps (after Lightfoot et al., 2012a, 2012b).

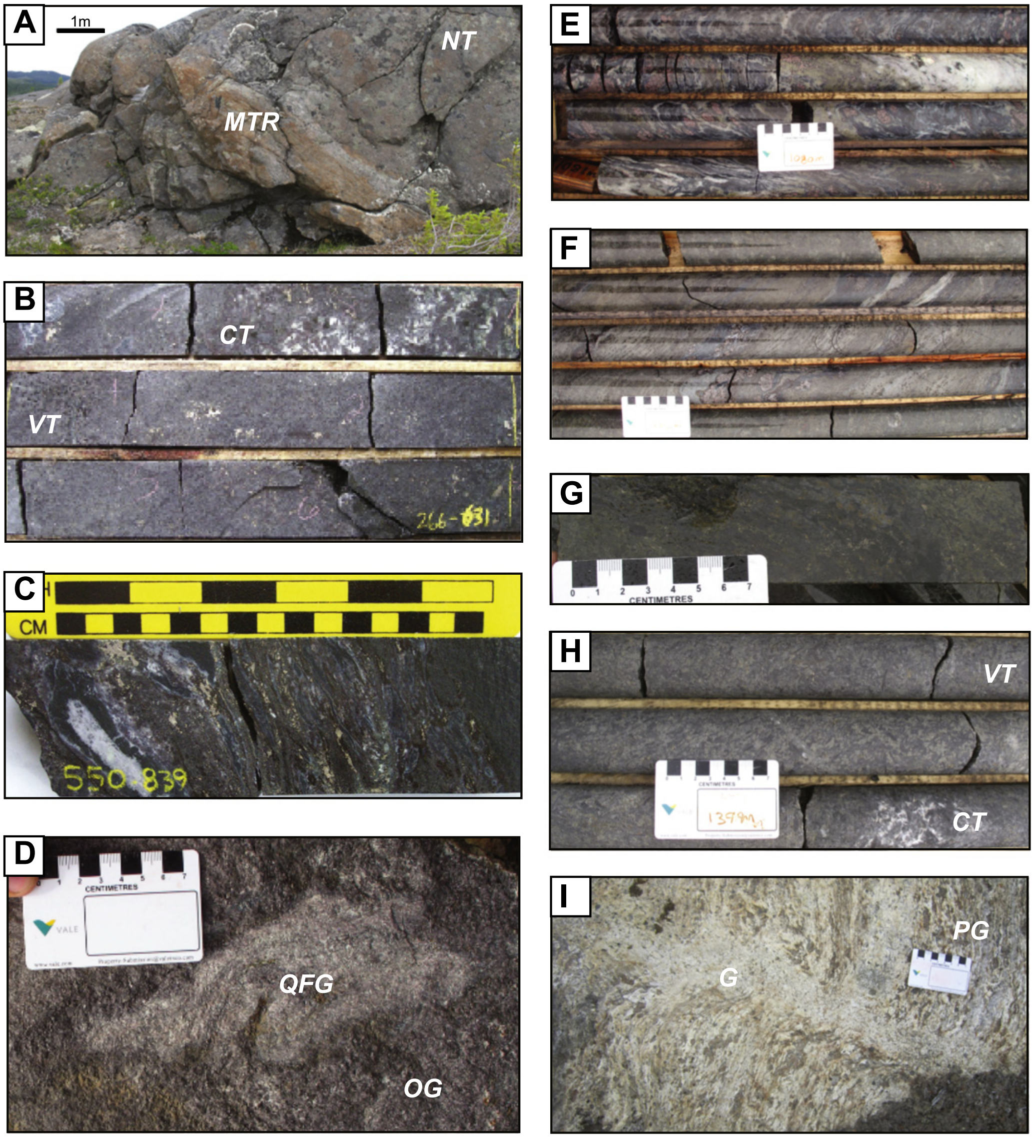

Fig. 17. A. Photograph showing a melatroctolite layer (MTR) in the normal-textured Troctolite (NT) of the Eastern Deeps Intrusion located ~400 m to the South of the surface projection of the Eastern Deeps Deposit. B. Variable troctolite (VT) of the Eastern Deeps showing extensive assimilation of orthogneiss; contaminated Troctolite (CT) is typically developed adjacent to Nain orthogneiss pendants within the Eastern Deeps Intrusion; sample comes from drill core VB266 at a depth of 631 m). C. Interface between low and high Ni tenor sulfides above the Eastern Deeps Deposit; this layer often comprises a condensed breccia sequence where aspect ratios are ~10–20 and the flat structures are associated with inclusions, mica, amphibole, and chlorite. The core comes from drill core VB550 at a depth of 839 m. D. Assimilation of quartzofeldspathic gneiss (QFG) in olivine gabbro (OG) at the northern margin of the mini-Ovoid. E. Country rock paragneisses adjacent to the Western Deeps Intrusion (VB459, 1080 m), showing textures indicative of incipient partial melting and genesis of inclusions that typify the breccia sequence rocks of the Voisey's Bay Deposit. F. Strongly banded paragneiss with incipient development of textures and mineralogies typical of paragneiss inclusions in the Voisey's Bay Deposit; core comes from country rocks adjacent to the Western Deeps Intrusion (VB459, 142 m). G. Variable-textured troctolite of the Western Deeps Intrusion with inclusions of paragneiss and weak disseminated Ni–Cu sulfide mineralization (VB98-459; 1444 m). H. Variable-textured Troctolite (VT) with evidence for in-situ assimilation of paragneiss fragments (CT); I. Folding of country rock paragneiss (PG) and emplacement of granitoid (G) magma along dextral shears which trends NNE developed west and south of the Reid Brook Zone.

heavily modified the troctolites by re-setting the U–Pb systematics of 1.334 Ga zircons in the troctolites to the ~1.306 Ga ages of the granitoid rocks (Amelin et al., 1999, 2000). The granites broadly occupy a similar footprint to mafic igneous rocks and they have a sheet-like geometry similar to the mafic intrusions; it appears likely that a similar stress regime controlled the distribution of magmatic activity at Voisey's Bay for approximately 30 Ma.

The flat alignment fabrics in the dyke and intrusion point to an alignment of inclusions in response to a stress regime that controlled the influx of magma and sulfide through the conduits and into the chamber. The relationships between mineralized mafic rocks and barren mafic rocks are generally quite complex, with no knife-sharp contacts between normal troctolite and variable-textured troctolite in the Eastern Deeps Intrusion, or between barren olivine gabbro or troctolite and the mineralized sequence in the dyke, so the geological evidence points to an episodic development of the chamber on a time scale consistent with partial crystallization. The relationships between barren mafic rocks, mafic rocks with disseminated mineralization, and inclusion-packed semi-massive to massive sulfide appear to be in this sequence, with the last event comprising the migration of the sulfide- and fragment-laden batches of magma along widened pathways within the dyke into gently dipping structural spaces where they accumulated. The interface in Ni tenor between heavily mineralized and weakly mineralized parts of the Eastern Deeps appears to support the earlier introduction of magma carrying disseminated sulfide into a chamber and the later introduction of massive sulfide and breccia sequence rocks (Fig. 19A).

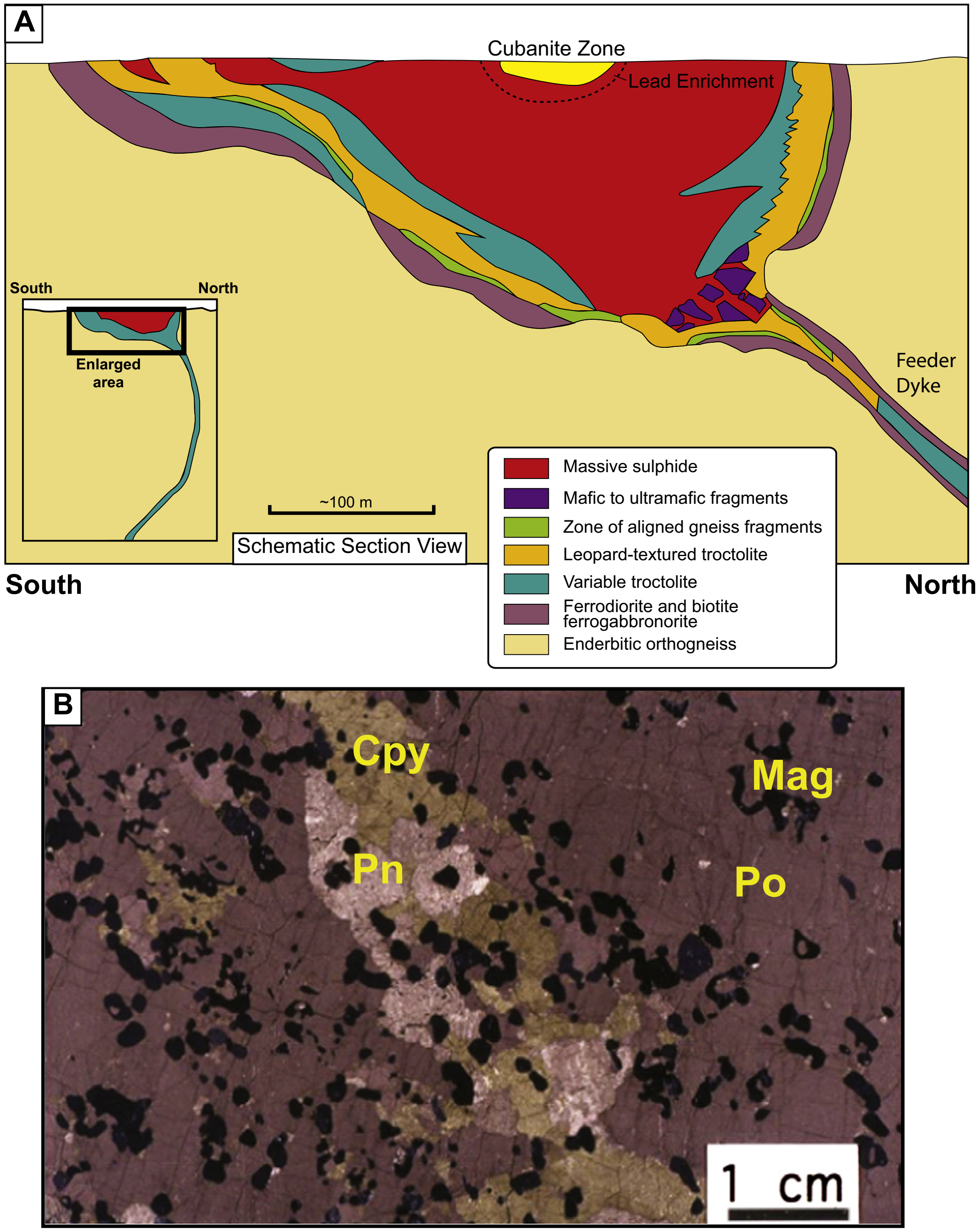

Fig. 18. A. Simplified geological cross section of the Ovoid Deposit showing key geological relationships. B. Massive Ni–Cu–Co sulfide mineralization from the Ovoid Deposit.

4.4. Internal form and structure of the Ovoid and the Reid Brook Zone

West of the Eastern Deeps chamber, the dyke bifurcates, and the upper part of the dyke is connected into an east–west trending elongated bowl-shaped intrusion termed the Ovoid (Figs. 15B–C and 18A). The core of the Ovoid comprises massive sulfide with resorbed magnetite (Fig. 18B); the massive sulfide is entirely devoid of gneiss fragments, but the margins have similar rock types to those developed around the Eastern Deeps, including both leopard-textured troctolite and breccia sulfides. The shape of the space occupied by the Ovoid Deposit is broadly an elongate west–east trough with a dyke connected to the base as a keel which dips to the north. The north wall of the Ovoid curves towards the south at the east end of the trough, and the south wall curves towards the north at the west end, so the geometry is broadly consistent with the space created by both rifting (Cruden et al., 2008) and at a cross-linking structure along a right-stepping dextral fault system (Lightfoot and Evans-Lamswood, 2014).

Further to the west, the Ovoid narrows into the mini-Ovoid deposit where the chamber walls are steeper, and the deposit is contained in an intrusion that has a wine-glass shape with a narrow keel (Evans-Lamswood et al., 2000). West of the Ovoid, the intrusion has the form of a dyke which dips towards the north, steepening with depth before bending over and dipping towards the south. The axis of the inflection of the dyke plunges east at ~27°, and the inflection reaches the surface in the Reid Brook Zone to the west of the Mini-Ovoid (Fig. 20). The dyke is variable in width (5–100 m) and discontinuous on the scale of 10–200 m. The wide parts of the dyke plunge at 45° to the east, and typically contain heavy Ni–Cu sulfide mineralization with magmatic breccias (Fig. 21A).

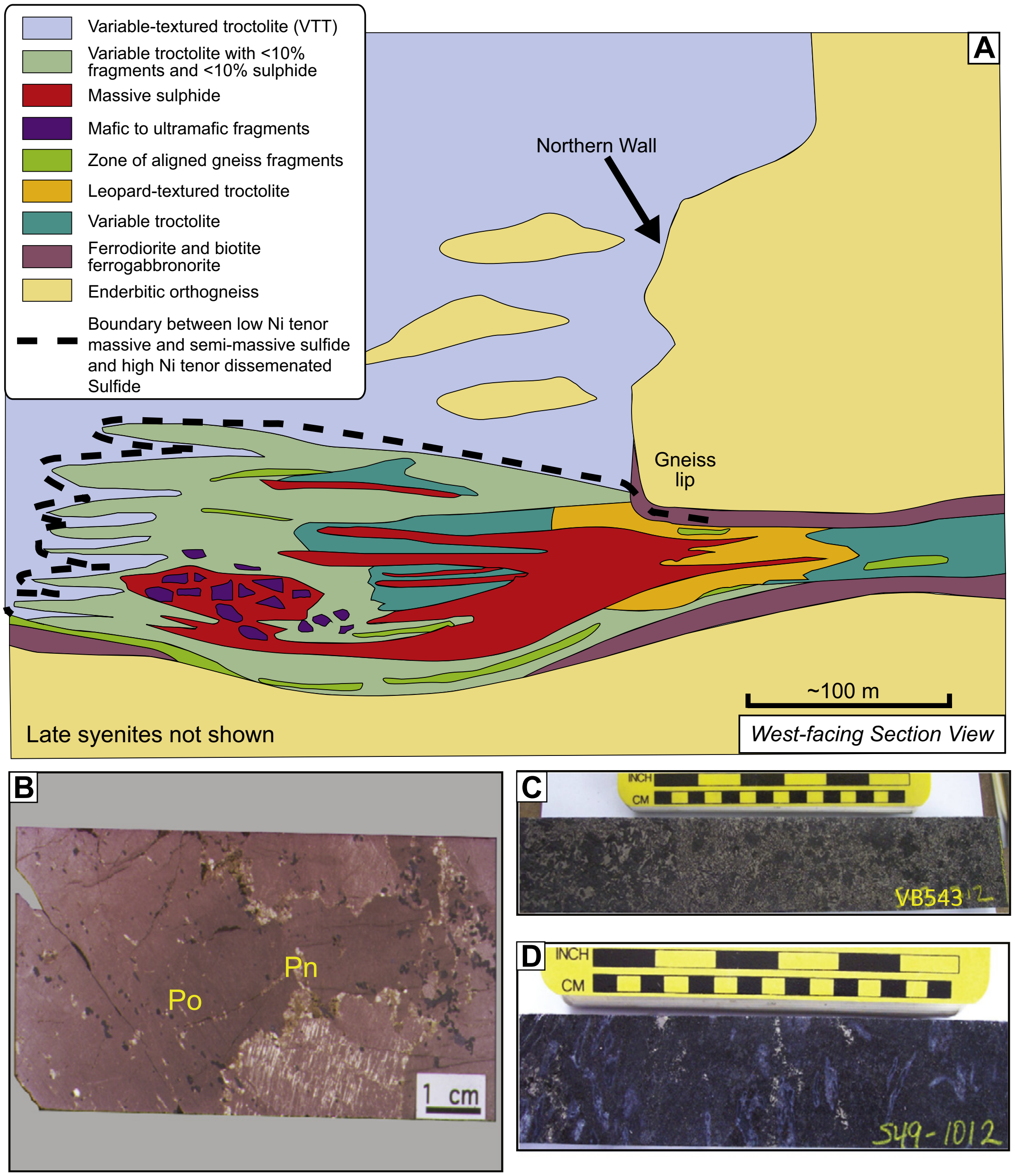

Fig. 19. A. Geological model showing the distribution of the range of silicate rock types, inclusions, and sulfides developed in the Eastern Deeps Deposit (modified after Lightfoot and Naldrett, 1999). Location of the model is shown in Fig. 15B. B. Massive Ni–Cu sulfide from the Eastern Deeps Deposit. C. Leopard-textured troctolite from the Eastern Deeps Deposit. D. Breccia sequence rocks with variable-textured troctolite from the Eastern Deeps Deposit.

The dyke follows the south side of the Western Deeps Intrusion (Fig. 21B). Although the dyke is adjacent to the south wall of this chamber, it is not entirely clear whether the dyke joins with the chamber or just skirts the south-dipping southern margin of the chamber because the contacts are normally cut by late granitoid intrusions (Lightfoot et al., 2012a, 2012b).

A zone of mineralization at the western end of the dyke comes near to surface, and is hosted partially by a widened zone of variable-textured troctolite inside the dyke, and partially along eastward-plunging sheet-like structures that slightly offset the dyke (upside to the north), and contain massive sulfides of similar composition to those found in the dyke (Lightfoot et al., 2012a,b). This domain contains the Reid Brook Deposit, and the broad envelope of this complex zone plunges from west to east at about 27° within the dyke as shown on the long section in Fig. 15C. The dyke extends from surface to depth along a plane which plunges to the north near-surface, bends over to a vertical orientation with depth, and then plunges towards the south at about 70° at depth as shown in the 3D model in Fig. 16. The dyke intersects a chamber of olivine gabbro, troctolite, ferrogabbro, and leucogabbro at depth that is termed the Western Deeps Intrusion. Within the stratigraphy of the Western Deeps Intrusion are intercalations of Tasiuyak Gneiss in which there are incipient metamorphism and partial assimilation of paragneiss to form the fragments that typically occur in association with the disseminated and breccia style Voisey's Bay sulfide ores (Fig. 18E–F). Nearby olivine gabbro and troctolites of the Western Deeps contain paragneiss inclusions, partial melts that appear to be derived from the gneiss and disseminated sulfide (Fig. 17G–H).

Geological relationships in the mineralized part of the dyke are summarized in Fig. 21A–B. The wide zones of stronger mineralization associated with magmatic breccias tend to plunge down the dyke towards the east with a rake of about 27°. Above the wider channel in the dyke, the dyke often narrows or is absent; in many cases the only manifestation of the dyke is massive sulfide (Fig. 21C–D). The sulfide

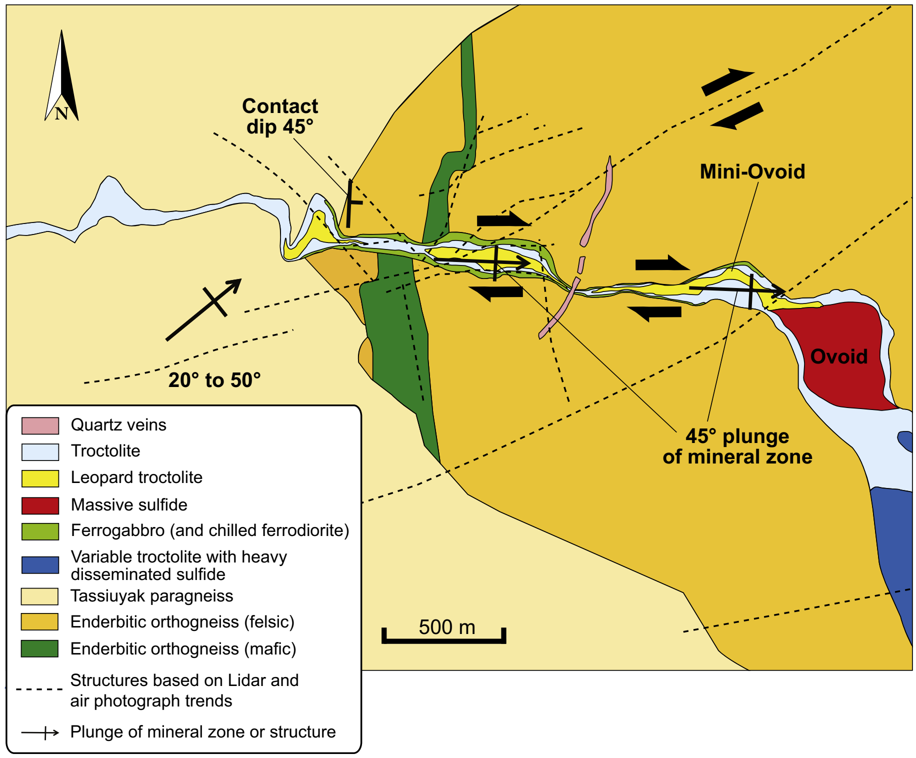

Fig. 20. Geological map of the Reid Brook dyke west of the Mini-Ovoid; map shows the distribution of mapped rock types and the location of main faults and structural features from an image of Lidar bare-earth digital elevation data.

lenses follow structures that dip to the east at 20–30°. It is these structures that appear to represent primary discontinuities in the dyke along which sulfide magmas (devoid of silicate melt and inclusions) have been injected into the country rock paragneiss (Fig. 21C–D). The country rocks adjacent to the dyke develop shear zones with evidence to further support dextral motion (Figs. 17I and 20). The sub-horizontal structures allowed migration of massive sulfide into the adjacent country rock gneisses as shown in Fig. 21A and C.

4.5. A refined model for the emplacement of the VBI and the associated Ni–Cu–Co sulfide mineralization

The geological relationships summarized above point to a protracted evolution of the crust in the area of the Voisey's Bay Deposit. The host intrusion appears to have been emplaced into a segment of crust that was undergoing extension. The geological evidence points to the presence of at least two main chambers in the structural corridor, the Eastern Deeps and the Western Deeps connected by a dyke (Evans-Lamswood, 2000; Lightfoot and Naldrett, 1999; Fig. 22A). The evolution of this chamber has been considered to be the product of caldera collapse within a west–east rift (Cruden et al., 2008) based on the structural setting, and this model has been widely used to explain the redistribution of dense magmatic sulfides and fragment laden melts from deeper chambers to shallower chambers in the crust (e.g. Lightfoot et al., 2012a,b; Fig. 22A).

Although our data from Voisey's Bay indicate that the morphology of the intrusion has been affected by collapse within a rift structure, there is also a growing weight of evidence that points to the presence of cross-linking structures as an important control on the development of wider segments of the conduit during dextral displacement along the E–W fault system. The plunging pipe of mineralization within the dyke, and the associated openings in the gneisses where the dyke is thin are small-scale manifestations resulting from transtensional slip that is recorded by <~100 m displacements in lithologic units across the dyke. The introduction of dense magmatic sulfides through this plumbing system would be a response to lateral tectonic pumping of sulfides rather than vertical transport of entrained sulfides in a flowing magma (De Bremond d'Ars et al., 2001). The origin of the spaces occupied by the mini-Ovoid, Ovoid, and Eastern Deeps chambers remains the subject of ongoing studies, but it appears likely that a combination of rifting and dextral faulting has created the conditions for the development of the Ovoid and the Eastern Deeps in a segment of the fault system by scissor faulting as shown in the block model in Fig. 22B.

5 . Discussion

5.1. Global examples of structural control on magma chamber geometry

A number of significant Ni deposits are associated with chonoliths that broadly resemble the Noril'sk–Kharaelakh, Voisey's Bay and Chinese Ni deposits. In South Africa, the 2.055 Ma Nkomati (Uitkompst) deposit is associated with an intrusion that is co-magmatic with the Rustenburg Layered Series of the Bushveld Intrusion (de Waal et al., 2001; Maier et al, 2004). The intrusion has a cross section morphology that broadly resembles the Talnakh Intrusion and Kalatongka, but the strongly differentiated intrusion is contained within and appears to have replaced the stratigraphy of the Transvaal Group.

The 2.04–2.08 Ga Voronezh Intrusions in SW Russia (Chernyshov, 2004) have a similar age to Nkomati (see above), and were likely originally part of an adjacent block of the Kapvaal Craton. These intrusions are only described from drill core, but the extent of differentiation and sulfide/silicate ratios may make them similar examples of Bushveld-related magmatism.

The 1.1 Ga Mid-continent Rift of North America contains a thick sequence of basaltic rocks within the main rift, and at the margins of the rift are major gabbro-anorthosite intrusions that are associated with Cu–Ni–PGE sulfide mineralization (e.g. parts of the Duluth Complex), but a particular group of intrusions developed inboard of the main rift during early extensional ultramafic magmatism are known to host Ni–Cu–PGE sulfide mineralization. These intrusions include Eagle in

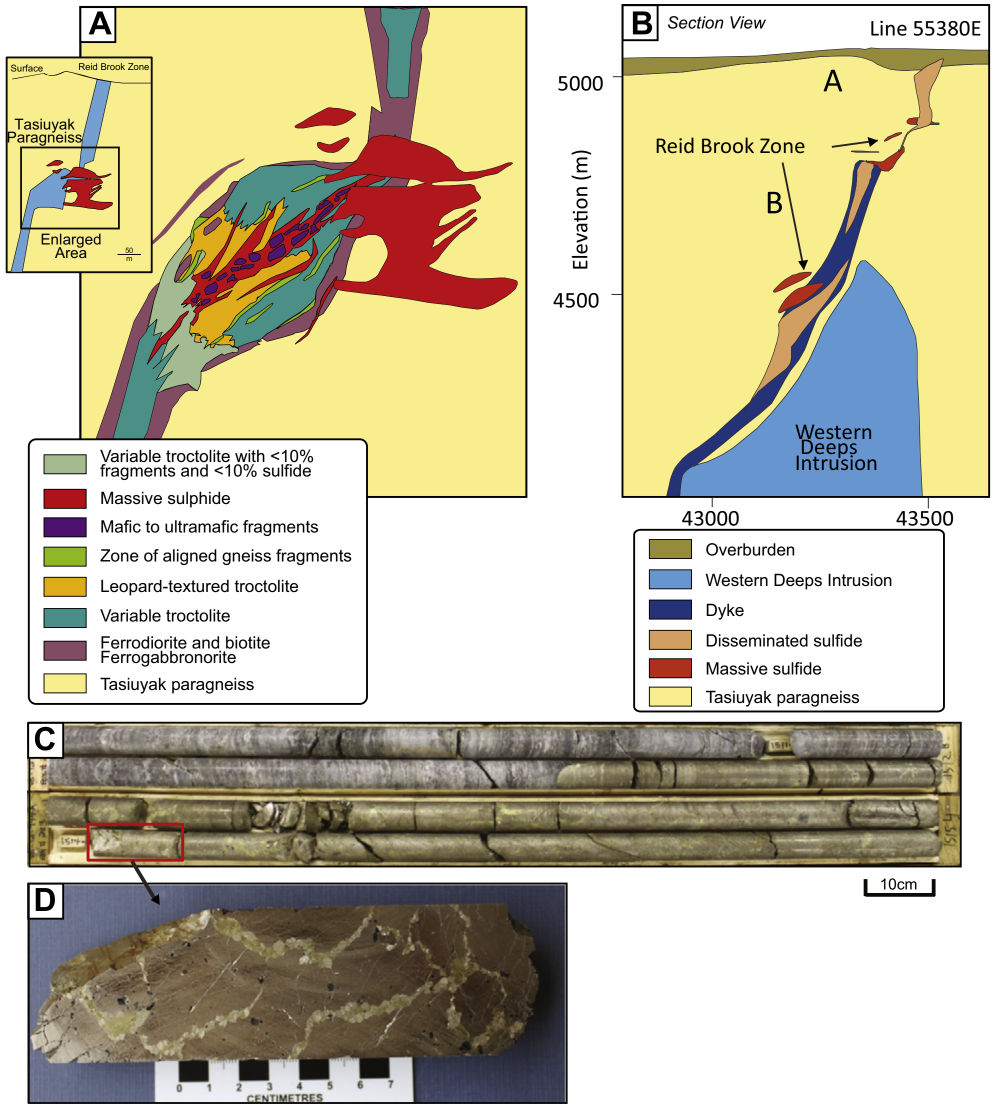

Fig. 21. A. Geological section through the western part of the Reid Brook Zone, showing the development of massive sulfides in adjacent gneisses and zones of mineralized troctolite and olivine gabbro in wider zones of the dyke; based on drill core data and surface mapping (modified based on more recent drilling from Lightfoot and Naldrett, 1999). B. Detailed geological relationships in the Reid Brook Zone sulfide zones which extend into the country rocks away from a narrow segment of the dyke; C. Massive sulfide vein hosted in country rock paragneiss of the Reid Brook Zone. D. Massive sulfide from the Reid Brook Zone (drill hole VB12-944A at 1514 m); the sulfides comprise large pyrrhotite crystals with some ex-solution lamellae of pentlandite, surrounded by thin loops of chalcopyrite with granular pentlandite (termed loop texture).

Michigan (Ding, 2011), Tamarack in Minnesota (Goldner, 2011), Current Lake in Ontario (Goodgame et al., 2010), the Great Lakes gabbro intrusion (Cogulu, 1993), and other mafic–ultramafic intrusions at the rift margin (Smyk and Hollings, 2009). The 1.107 Ga Eagle deposit is a good example of a primitive funnel-shaped intrusion possibly associated with a splay of the Great Lakes Tectonic Zone; the size, morphology, internal differentiation and sulfide/silicate magma ratio are all comparable to the cluster that define many of the Chinese deposits. The Tamarack Intrusion in Minnesota within the broad trend of the Great Lakes Tectonic Zone; this 1.106 Ga intrusion is also quite small in plan, and appears to occupy a bridging structure between intrusions developed in a splay of the Great Lakes Tectonic Zone. Relative to Tamarack, there is a larger body of information on the Current Lake Intrusive Complex north of Thunder Bay. This intrusion is strongly differentiated, and comprises many dyke-like segments that are within splays of the Quetico Fault Zone, but bridging structures extend between the dykes which form channels containing disseminated PGE–Ni–Cu sulfide mineralization (Goodgame et al., 2010). The Great Lakes Nickel Deposit is another example of differentiated intrusion with disseminated sulfide mineralization (Cogulu, 1993); the exact configuration of the intrusion is not completely understood, but it does appear to rest at the western termination of a dyke-like composite intrusion of gabbros and granophyres that has been termed the Mollie-Pine River Intrusion (Sutcliffe, 1987). It is possible that this intrusion is a lateral extension of this dyke.

Conduit style intrusions are not restricted to the Phanerozoic and Proterozoic; the 2734 Ma Eagle's Nest intrusion in the "Ring of Fire" in NW Ontario is an example of an Archean champagne-glass shaped intrusion that resides within a broad structural zone and is strongly differentiated (Mungall et al., 2010). Elevated sulfide/magma ratio is also a feature of this body. It is possible that other small Archean-aged and Proterozoic intrusions share similarities to the chonoliths described above, but are more heavily deformed in comparison. Examples include the 1.97 Ga Pechenga Deposits, where the small intrusions are associated with large volumes of magmatic sulfide (Green and Melezhik, 1999; Lightfoot et al., 2012a; Laverov, 1999)

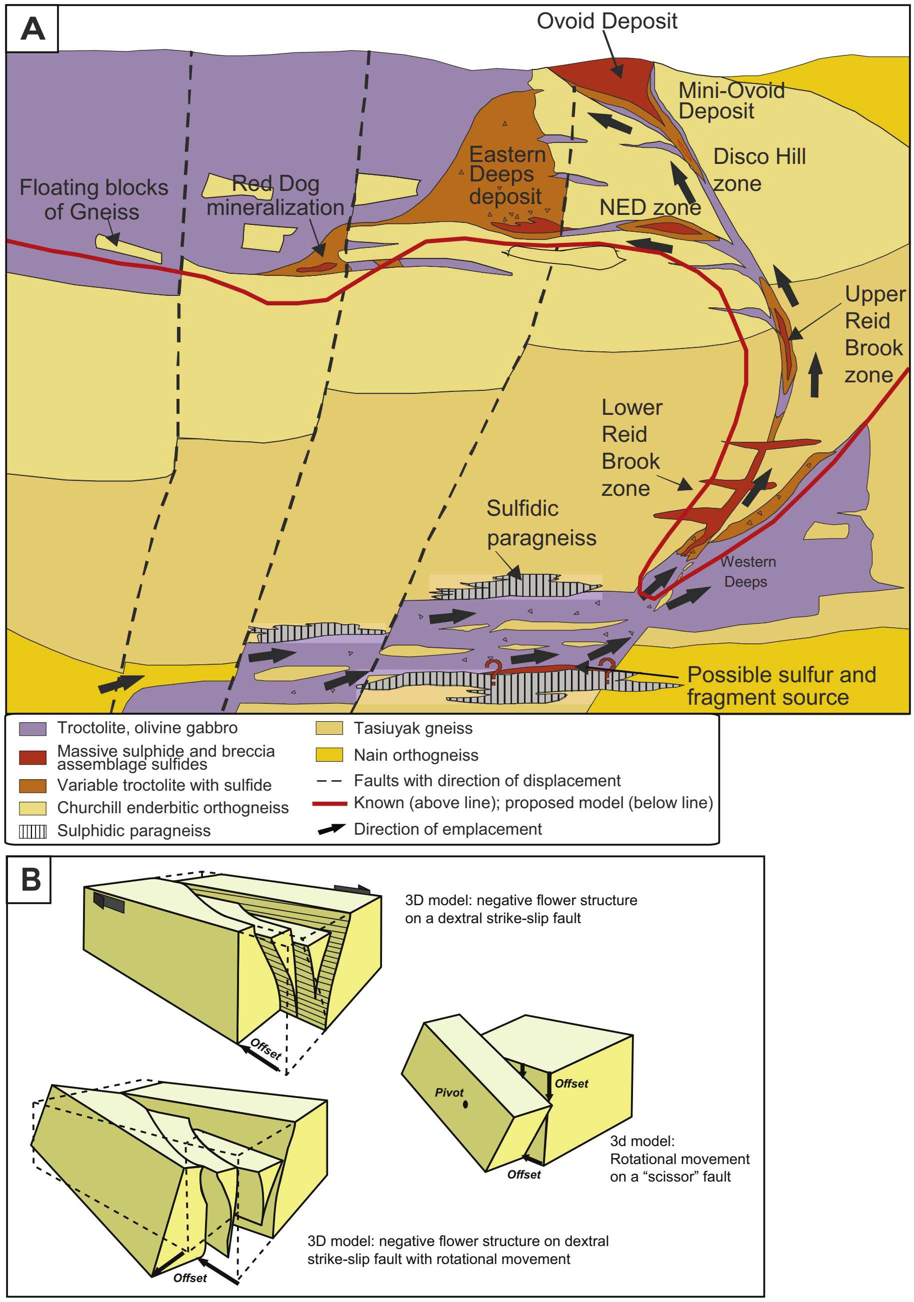

Fig. 22. A. Geological model for the Voisey's Bay deposit showing geological relationships from west to east across the deposit condensed into a single west-facing section (after Lightfoot et al., 2012a, 2012b). Information available from drilling is shown above the red dotted line; below this line, the diagram depicts a possible model. B. Schematic 3D block models showing how a combination of rotational movement on a scissor fault combined with dextral strike-slip motion creates the differing geometry of the Eastern Deeps chamber and the Discovery Hill dyke (after Lightfoot and Evans-Lamswood,2012, 2013, 2014).

and the 1.87 Ga Thompson Deposit in the Thompson Nickel Belt of Manitoba (Lightfoot et al, 2012c). Another example may be the 1.4 Ga Kabanga Deposit in Tanzania (Maier et al., 2010), where the small intrusions have geometries remarkably similar to those that host mineralization at Pechenga.

In Western Australia, two key examples of chonoliths with sulfide mineralization are developed. In the Halls Creek Orogen, the 1.88 Ga Sally Malay (Savanah) Intrusion hosts mineralization in a small conduit that strongly resembles the Voisey's Bay deposit in petrology, inclusion-sulfide associations, and shape (Page and Hoatson, 2000; Thornett, 1981). Another example in the West Musgrave Block is the 1078 Ma Babel–Nebo Intrusion which is a very small differentiated chonolith that contains a lower segment that is strongly enriched in disseminated sulfide. Seat et al (2007, 2009) describe the detailed geology of this intrusion, and the geological relationships summarized in their sections share many similarities with the more weakly mineralized segments of the Noril'sk and Kalatongke Intrusions described above.

Although there are many examples of economically or sub-economically mineralized small intrusions, there are also many examples which are barren of mineralization or barren at the present level of erosion. Although structural controls are of primary indicator of exploration potential, there are many other features in common in these intrusions (Table 1), and a wide range of other process controls which govern the formation of magmatic Ni–Cu–Co–(PGE) sulfides within chonoliths (e.g. Lightfoot, 2007; Naldrett, 2010).

5.2. Comparative geology of the Offset Deposits of the Sudbury Igneous Complex

Some of the Ni–Cu–PGE sulfide deposits associated with the Sudbury Igneous Complex (SIC) in Ontario, Canada share features of the dyke-hosted mineralization at Voisey's Bay. The strongest analogy exists for a group of deposits which are associated with radial dykes of quartz diorite which extend away from the main Sudbury Igneous Complex into the country rocks. These are traditionally termed Offset Dykes, and they contain very large ore deposits (e.g. the ore deposits of the Copper Cliff Offset). The geology of these dykes and their relationship to the SIC are described in Lightfoot et al (1997a,b,c, 2000), and Keays and Lightfoot (2004). The dykes appear to have formed early in the evolution of a melt sheet generated by meteorite impact (Grieve, 1994). The Offset dykes are radiating structures in the crust which were initially filled with undifferentiated magma with the bulk composition of the average SIC melt (Lightfoot et al., 199). The Main Mass magma achieved S saturation, and sulfide-laden magmas together with inclusions were injected into the Offset dykes from above to form steeply plunging ore shoots. These mineral zones tend to be localized in places where the dyke is thick (Farrow and Lightfoot, 2000; Lightfoot and Farrow, 2003), and often adjacent to primary discontinuities in the dyke which are often located in areas of extensive country rock brecciation (e.g. Farrow and Lightfoot, 2000; Lightfoot, 2007). The localization of the mineralization in these dykes appears to be controlled by local cross structures between faults developed radially and concentrically around the SIC. A close analogy exists between the geometry of the Reid Brook Zone at Voisey's Bay and the mineral zones of the Copper Cliff and Worthington Offset which are part of the Sudbury Igneous Complex.

5.3. A new model for a class of nickel deposits in intrusions linked to strike-slip structures

An important feature of the Earth's crust is the extensive long-lived network of strike-slip faults which are a kinematic product of motion of the plates which comprise the Earth's crust (Wilson, 1965). Strike-slip faults can occur in a range of settings (Cunningham and Mann, 2007), but most critically to the context of the formation of small intrusions in cratonic margin settings, the strain developed during passive rifting or plume-initiated active rifting appears to generate deep rooted structural zones which sometimes control the migration of magma from the mantle to the surface.

Rifting is an important process in the context of crustal thinning, and provides an opportunity for mantle-derived magmas to migrate from mantle to surface. Strike-slip faults comprise a sub-set of structures which typically develop in response to anisotropy of the motion of plate margins. The structures associated with strike-slip motion include both restraining and releasing bends. Within areas of transpression, positive flower structures are indicative of the sense of transpression and may have manifestations like en echelon folds in adjacent sedimentary stratigraphy; there is no opportunity for structural space to be generated which can be exploited by ascending magma. In contrast, releasing structures at sites of transtension may take the form of transtensional rifts and pull-apart basins where the detailed internal geometry of motion of blocks within the rift or pull-apart has a vertical and lateral sense of displacement. Transtension generates local open space in the crust, and sub-vertically connected open spaces provide a pathway through which mantle-derived magmas can migrate from the mantle to the crust. Such pathways would tend to focus on the margins of active rifts and reflect far-field rather than local stress regimes in the development of en echelon shears. Transtensional space is created in response to country rock anisotropy, and so the spaces would tend to occur in different locations along a fault structure, but may be physically connected at the lower and upper ends into vertical and lateral shear zones. The pathway followed by this magma in a complex strike-slip fault zone is unlikely to be a simple dyke-like geometry as the domains of transpression will inhibit migration of magma whilst the zones of transtension will promote the episodic movement of magma. The geological relationships documented in many of the intrusions with a funnel-shaped cross section and a rhombic plan outline (e.g. Huangshan, Huangshandong, Limahe, Voisey's Bay) are consistent with the development of the magma chambers and conduits through local transtension. The morphology of this space reflects anisotropy in the country rocks, and so the closure of the pull-apart would be both below and above the opening. To allow magma to enter these rhombic openings in the strike-slip structure, an interconnected network of open space is required (Lightfoot et al., 2012a), and this may take the form of both vertical pipe-like segments in the lower and upper tails of the intrusions, much like the dykes found at Voisey's Bay, Jinchuan, and Hongqiling. Anisotropies may also be horizontal and sub-horizontal, and this can give rise to lateral flow of magma along conduits between larger transtensional spaces; in this case, the magma channels resemble the oblate conduits recognized in the Noril'sk I, Talnakh, and channel-ways in the Kharaelakh Intrusion. More oval-shaped pipe-like intrusions include the examples from Kalatongke, Babel–Nebo, and Nkomati.

5.4. Significance of large igneous provinces, cratonic margins, and supercontinent break-up

The extent to which magma can easily transfer from mantle to crust is controlled by the efficiency of maintenance of an open conduit system. During incipient rifting, the magmas generated within many large igneous provinces are typically more primitive and limited in volume. This is illustrated by the volumetrically small contributions of Gudchikhinsky picritic basalts to the lower part of the Siberian Trap at Noril'sk, and by the presence of picritic basalts in the basal stratigraphy of the Keweenawan Mid-Continent Rift at Mamainse Point (Berg and Klewin, 1988) and the Osler Volcanic Group (Keays and Lightfoot, in preparation). In the case of the Mid-continent rift, intrusions that are broadly coeval and potentially co-magmatic with picritic basaltic rocks include Eagle and Tamarack which were emplaced during incipient rifting. These phases of early rifting allowed a magma transportation network to develop in favorable structures at the cratonic margin. It is the cratonic margin that is typically composed of thinner lithosphere, and through which magma can more readily migrate from the mantle to the surface during the early active rifting phase of continent break-up (Begg et al., 2010).

In the context of heat flow and continent dis-amalgamation, the phase of activity immediately following the development of a superplume appears to be a critical temporal event for the formation of nickel sulfide deposits. There is a marked increase in the quantity of mineralized mafic and ultramafic rock immediately following the break-up of Kenorland, Nuna, Rodinia, and Pangea as evidenced by the correlation between contained Ni in historic resources and future production versus the age of the host intrusion (Maier and Groves, 2011). The onset of dis-amalgamation follows periods of maximum addition of juvenile crust (Bradley, 2011), and the majority of nickel deposits link to the large igneous province events that follow break-up.

5.5. Magma dynamics in conduit systems

Most of the intrusions within cratonic margin structures have similar features, including: 1. Ultramafic and mafic rock types; 2. geological evidence for the equilibration of the magma with crust or inclusions of crustal derivation; and 3. the intrusions are endowed with accumulations of magmatic sulfides that are enriched in Ni, Cu, and Co, and sometimes PGE. The extent to which economic concentrations of mineralization link to the presence of inclusions varies between different deposits. At Voisey's Bay, there is a close empirical association between disseminated sulfides, olivine gabbro and troctolite, and the presence of paragneiss fragments and ultramafic inclusions; this association is more typical of the halo around massive sulfide veins systems where ore bodies like the Eastern Deeps and the Ovoid are essentially barren of inclusions within the massive sulfide veins which appear to cross-cut the earlier mineralized breccia sequence rocks. In contrast, the Noril'sk–Talnakh Deposits comprise disseminated sulfides which locally have inclusions of fine-grained black metasedimentary material in taxitic gabbronorites (Lightfoot and Zotov, 2007, 2014), but the massive Ni-rich ore veins are devoid of inclusions as well as segregations of gabbroic melt; these veins appear to have been injected late, and the abundance of the veins in the footwall is indicative of quite late introduction into the Kharaelakh and Talnakh Intrusions. These associations led Lightfoot et al. (2012a, 2012b) to suggest that the Voisey's Bay sulfides were injected into their final resting place in a series of variably sulfide-enriched pulses (Fig. 22). Likewise, we speculate that the Noril'sk mineralization was emplaced late in the evolution of the magma channel-way, and was not the product of in-situ upgrading of sulfide in Ni, Cu, and PGE produced by passing batches of silicate magma equilibrating with the sulfide (e.g. Naldrett et al., 1995). The high ratio of sulfide/magma found in mineralization with elevated metal tenor in 100% sulfide provides additional evidence for emplacement of sulfide melts for the other intrusions discussed in this paper. Some of these intrusions have ratios of sulfide/magma of ~1 (e.g. Hongqiling Number 7 Deposit), whereas other intrusions like Jinchuan have ratios of 0.02 which are still remarkably high, and inconsistent with in-situ generation of the high Ni tenor mineralization.

Emplacement of magmas through a trellis of magma conduits and chambers developed in transtensional segments of strike-slip structures offers a context in which to better understand sulfide transport. Voisey's Bay represents a case example where the emplacement of sulfide magma appears to follow structures which plunge up the axis of the dyke at roughly 40°. In the case of Noril'sk, the chonoliths have a very gentle dip parallel to the Noril'sk–Kharaelakh Fault, and the principal mineral channels follow the thickest parts of the chonolith along these gently (~10°) plunging magma conduits. In the case of the Chinese deposits, the principal pathways are associated with sub-vertical mantle-penetrating structures. Transportation of massive sulfide through vertical conduits has been shown to be unlikely based on the density and viscosity relationships between silicate and sulfide magma (de Bremond d'Ars et al., 2001); the presence of gently plunging channels with staging chambers offers an alternative to this paradigm, and one that explains the range in examples described in this study.

6 . Summary and conclusions

Many examples of small differentiated mafic–ultramafic intrusions with significant Ni–Cu–PGE sulfide deposits are associated with major crustal structures. The following examples share common features including the creation of space adjacent to fault zones by local structures that link into mantle-penetrating fractures which have localized magmatism in the roots of large igneous provinces (e.g. Lightfoot and Evans-Lamswood, 2013, 2014).

1. *Diamond-shaped plan and funnel-shaped cross section*. Examples of intrusions with nickel sulfide deposits are Jinchuan, Hongqiling Number 1, Jingbulake, Kalatongke, Huangshan, Huangshandong, Limahe, Qingquanshan, Lengshuiqing, Zhubu, Ban Phuc, the Ovoid, Discovery Hill, Eastern Deeps, Eagle, Double Eagle, Aguablanca, Maksut, Santa Rita, and Suwar
2. *Pipe-like geometry*. Examples of intrusions with nickel sulfide deposits are Baimazhai, Tongdongzi, Talnakh, Kharaelakh, Noril'sk I, Noril'sk II, Chernagorsk, Maslovskoe, Tamarack, Current Lake, Babel–Nebo, Nkomati, Limoeiro, Chibasong, Wellgreen, and Voronezh.
3. *Widened pipe-like conduits within dykes and structural discontinuities in dykes*. Examples of dykes with nickel sulfide deposits are the Reid Brook and Eastern Deeps dykes at Voisey's Bay, the Worthington and Copper Cliff Offsets of the Sudbury Igneous Complex, and the Hongqiling Number 7 Intrusion in China.

We recognize a number of features of a class of small strongly differentiated intrusions hosting Ni-sulfide deposits, viz: 1. A spectrum of Ni sulfide ore deposits are found in small intrusions with rhomboid-shaped outcrop patterns and funnel-shaped cross sections, narrow magma tubes, or within widened domains in dykes. Collectively we refer to these intrusions as chonoliths. 2. The volume of magma relative to the volume of sulfide in many small intrusions is too low to support the formation of the observed deposits by in-situ sulfide saturation and segregation. 3. The massive sulfide ore bodies are sometimes located in the country rocks adjacent to the intrusions (e.g. Talnakh) or choke the feeder conduits (e.g. the Ovoid Deposit); the formation of these deposits by upgrading of the metal concentration in an open system is not supported by geological relationships (e.g. Lightfoot and Zotov, 2014). 4. The small intrusions are often strongly differentiated with mafic and ultramafic rock types developed, and the Ni–Cu–PGE sulfide mineralization often has an elevated Ni tenor and a wide range in Ni/Cu ratio and PGE concentrations in sulfide. 5. The small intrusions tend to be spatially associated with regional structures that create space, and are localized by dilations and traps created by cross-linking structures in strike-slip fault zones.

We propose a model in which sulfide-laden magma ascended through a sub-vertical conduit system in a structural zone from a parental source/chamber at depth. The transportation of dense sulfide takes place through a conduit system undergoing transtension and transpression, which effectively pumps the sulfide through the conduit system. These structures are part of the tectonic framework in both large igneous provinces and anorogenic settings.

These controls may also have been important in controlling the original geometry and primary ore localization in intrusions that have been extensively modified by deformation and metamorphism; examples include the komatiite channels and sub-volcanic intrusions of the Yilgarn, Thompson, Pechenga, and Raglan Belts (Lightfoot et al., 2012c).

Acknowledgments

We recognize the contribution of the late Professor Igor Zotov to developing ideas on the origin of the Noril'sk ore deposits and his enthusiasm and conviction that magma conduits like those of the Noril'sk region are open system magma and fluid conduits. Rogerio Monteiro is thanked for pointing out and illustrating the global significance of structure in controlling the emplacement of magmas and the formation of Ni sulfide ore deposits. We acknowledge Vivian Feng for supporting efforts to understand the diversity in Chinese nickel deposit. Professors Tang Zongli, Wen Yuan Li, and Nie Feng Jun for their advice and expert scientific opinion on Chinese nickel deposits; we also thank Karfai Leung for extensive support in the field and for gathering information on the diversity of nickel deposits in China. Ian Fieldhouse and Lisa Gibson are thanked for perceptive input and suggestions that were used in the preparation of the revised manuscript. Careful reviews by Christina Wang and Ed Ripley are acknowledged. The exploration skills of the team of geologists who worked to generate the datasets that underpin the current understanding of the Voisey's Bay Intrusion and the associated ore deposits; special thanks go to Robert Wheeler, Scott Mooney, Miro Mytny, Glenn McDowell, Danny Mulrooney, Kim Morrissey, Charlene McCooeye-Spyrka, Krista Reddy, Sheldon Pittman, Crispin Pike, Jennifer Glasgow, Darrell Butt, Trevor Rice, Rod Smith, and Dan Lee. We thank Derek Wilton for many discussions on the geology of Voisey's Bay. The drafting skills of Alex Gagnon are acknowledged. Permission from Vale to publish this paper is acknowledged.

References

Amelin, Y., Li, C., Naldrett, A.J., 1999. Geochronology of the Voisey's Bay complex Labrador Canada by precise U–Pb dating of co-existing baddeleyite zircon and apatite. Lithos 47, 33–51.

Amelin, Y., Li, C., Valeyev, O., Naldrett, A.J., 2000. Nd–Pb–Sr isotope systematics of crustal assimilation in the Voisey's Bay and Mushuau intrusions Labrador Canada. Econ. Geol. 94, 815–830.

Barnes, S.-J., Lightfoot, P.C., 2005. Formation of magmatic nickel sulfide ore deposits and processes affecting their copper and platinum group element contents. In: Hedenquist, J.W., Thompson, J.F.H., Goldfarb, R.J., Richards, J.P. (Eds.), Economic Geology 100th Anniversary Volume, pp. 179–213.

Begg, C.B., Hronsky, J.A.M., Arndt, N.T., Griffin, W.L., O'Reilly, S.Y., Hayward, N., 2010. Lithospheric, cratonic, and geodynamic setting of Ni–Cu–PGE sulfide deposits. Econ. Geol. 105, 1057–1070.

Berg, J.H., Klewin, K.W., 1988. High–MgO lavas from the Keweenawan midcontinent rift near Mamainse Point, Ontario. Geology 16, 1003–1006.

Bradley, D.C., 2011. Secular trends in the geologic record and the supercontinent cycle. Earth-Sci. Rev. 108, 16–33.

Chernyshov, N.M., 2004. Platinum-bearing Formations of the Kursk–Voronezh region. Voronezh State University, Voronezh (448 pp.).

Cogulu, E.H., 1990. Mineralogical and petrological studies of the Crystal Lake Intrusion, Thunder Bay, Ontario, Open File Report, 2277 Geological Survey of Canada.

Cogulu, E.H., 1993. Mineralogy and chemical variations of sulfides from the Crystal Lake Intrusion, Thunder Bay, Ontario. Geological Survey of Canada, Open File 2749 (52 pp.).

Cruden, A.R., Evans-Lamswood, D.E., Burrows, D., 2008. Structural, tectonic and fluid mechanical controls on emplacement of the Voisey's Bay troctolite and its Ni–Cu–Co mineralization. GAC Program with Abstracts, 33, p. 59.

Cunningham, W.D., Mann, P., 2007. Tectonics of strike-slip restraining and releasing bends. Geol. Soc. Lond. Spec. Publ. 290, 1–12.

de Bremond d'Ars, J., Arndt, N., Hallot, E., 2001. Analog experimental insights into the formation of magmatic sulfide deposits. Earth Planet. Sci. Lett. 186, 371–381.

de Waal, S.A., Maier, W.D., Gauert, C.D.K., Armstrong, R.A., 2001. Parental magma and emplacement of the stratiform Uitkomst Complex, South Africa. Can. Mineral. 39, 557–572.

Ding, X., 2011. Mineralogic, petrological and isotopic studies of the Eagle nickel–copper sulfide deposit, Michigan(PhD Thesis) University Indiana (158 pp.).

Ding, X., Li, C., Rpley, E.M., Rossell, D., Kamo, S., 2010. The Eagle and East Eagle sulfide orebearing mafic-ultramafic intrusions in the Midcontinent Rift System, upper Michigan: Geochronology and petrologic evolution. Geochemistry, Geophysics, Geosystems Volume 11 (Issue 3).

Evans-Lamswood, D.M. 2000. Physical and geometric controls on the distribution of magmatic and sulfide bearing phases within the Voisey's Bay nickel–copper–cobalt deposit, Voisey's Bay, Labrador Unpublished MSc thesis. Memorial University of Newfoundland. 212 pp.

Evans-Lamswood, D.M., Butt, D.P., Jackson, R.S., Lee, D.V., Muggridge, M.G., Wheeler, R.I., Wilton, D.H.C., 2000. Physical controls associated with the distribution of sulfides in the Voisey's Bay Ni–Cu–Co deposit Labrador. Econ. Geol. 95, 749–770.

Farrow, C.E.G., Lightfoot, P.C., 2000. Sudbury PGE revisited: toward and integrated model. In: Cabri, L.J. (Ed.), The Geology, Geochemistry and Mineral Beneficiation of Platinum-Group Elements. CIM Special Volume, 54, pp. 273–298.

Farrow, C.E.G., Watkinson, D.H., 1997. Diversity of precious-metal mineralization in footwall Cu–Ni–PGE deposits, Sudbury, Ontario: implications for hydrothermal models of formation. Can. Mineral. 35, 817–839.

Gao, J.-F., Zhou, M.-F., 2012. Generation and evolution of siliceous high magnesium basaltic magmas in the formation of the Permian Huangshandong Intrusion (Xinjiang, NW China). Lithos 162, 128–139.

Gao, J.-F., Zhou, M.-F., Lightfoot, P.C., Wang, C.Y., Liang, Q., 2012. Origin of PGE-poor and cu-rich magmatic sulfides from the Kalatongke Deposit, Xinjiang, Northwest China. Econ. Geol. 107, 481–506.

Glotov, A.I., Polyakov, G.V., Hoa, T.T., Balykin, P.A., Akimtsev, V.A., Krivenko, A.P., Tolstykh, N. D., Phuong, N.T., Thanh, H.H., Huang, T.Q., Petrova, T.E., 2001. The Ban Phuc Ni–Cu–PGE deposit related to the phanerozoic komatiite–basalt association in the Song Da Rift, Northwestern Vietnam. Can. Mineral. 39, 573–589.

Goldner, B., 2011. Igneous Petrology of the Ni–Cu–PGE Mineralized Tamarack Intrusion, Aitkin and Carlton Counties, Minnesota. University of Illinois (MSc thesis 156 pp.).

Goodgame, V.R., Johnson, J.R., MacTavish, A.D., Stone, W.E., Watkins, K.P., Wilson, G.C., 2010. The Thunder Bay North Deposit: chonolith-hosted Pt–Pd–Cu–Ni mineralization related to the midcontinent rift. 11th International Platinum Symposium. Abstract.

Green, A.H., Melezhik, V.A., 1999. Geology of the Pechenga ore deposits — a review with comments on ore forming processes. In: Keays, R.R., Lesher, C.M., Lightfoot, P.C., Farrow, C.E.G. (Eds.), Dynamic processes in magmatic ore deposits and their application in mineral exploration. Geol. Assoc. Can., Short-Course, vol. 13, pp. 287–328.

Grieve, R.A.F., 1994. An impact model of the Sudbury structure. In: Lightfoot, P.C., Naldrett, A.J. (Eds.), Proceedings of the Sudbury-Noril'sk symposium. Ontario Geological Survey Special Volume, 5, pp. 119–132.

Han, C.M., Xiao, W.J., Zhao, G.C., Qu, W.J., Mao, Q.G., Du, A.D., 2006. Re–Os isotopic analysis of the Kalatongke Cu–Ni sulfide deposit, Northern Xinjiang, NW China, and its geological implication. Acta Petrol. Sin. 22 (1), 163–170 (in Chinese).

Han, C.M., Xiao, W.J., Zhao, G.C., Su, B.X., Sakyi, P.A., Ao, S.J., Zhang, J., Zhang, Z., 2013. SIMS U–Pb zircon dating and Re–Os isotopic analysis of the Hulu Cu–Ni deposit, eastern Tianshan, Central Asian Orogenic Belt, and its geological significance. J. Geosci. 58, 251.

Hawkesworth, C.J., Lightfoot, P.C., Fedorenko, V.A., Blake, S., Naldrett, A.J., Doherty, W., Gorbachev, N.S., 1995. Magma differentiation and mineralization in the Siberian continental flood basalts. Lithos 34, 61–88.

Heaman, L.M., Easton, R.M., Hart, T.R., Hollings, P., MacDonald, C.A., Smyk, M., 2007. Further refinement to the timing of Mesoproterozoic magmatism, Lake Nipigon region, Ontario. Can. J. Earth Sci. 44, 1055–1086.

Kamo, S.L., Czamanske, G.K., Amelin, Y., Fedorenko, V.A., Davis, D.W., Trofimov, V.R., 2003. Rapid eruption of Siberian flood–volcanic rocks and evidence for coincidence with the Permian–Triassic boundary and mass extinction at 251 Ma. Earth Planet. Sci. Lett. 214, 75–91.

Keays, R.R., 1995. The role of komatiitic and picritic magmatism and S-saturation in the formation of ore deposits. Lithos 34, 1–18.

Keays, R.R., Crocket, J.H., 1970. A study of precious metals in the Sudbury nickel irruptive ores. Econ. Geol. 65, 438–450.

Keays, R.R., Lightfoot, P.C., 2004. Formation of Ni–Cu–platinum group element sulfide mineralization in the Sudbury impact melt sheet. Mineral. Petrol. 82, 217–258.

Keays, R.R., Lightfoot, P.C., 2009. Crustal sulfur is required to form magmatic Ni–Cu sulfide deposits: evidence from chalcophile element signatures of Siberian and Deccan Trap Basalts. Miner. Deposita 45, 241–257.

Kunilov, V.Ye, 1994. Geology of the Norilsk region: the history of the discovery, prospecting, exploration and mining of the Norilsk Deposits. In: Naldrett, A.J., Lightfoot, P.C., Sheahan, P. (Eds.), The Sudbury–Norilsk Symposium Ontario Geological Survey Special Publication, 5, pp. 203–216.

Laverov, N.P., 1999. Copper—nickel deposits of the Pechenga Region. Moscow Geos. 236.

Li, C., Lightfoot, P.C., Amelin, Y., Naldrett, A.J., 2000. Contrasting petrological and geochemical relationships in the Voisey's Bay and Mushuau intrusions, Labrador, Canada: implications for ore genesis. Econ. Geol. 95, 771–801.

Li, C., Ripley, E.M., Maier, W.D., Gomwe, T.E.S., 2002. Olivine and sulfur isotopic compositions of the Uitkomst Ni–Cu sulfide ore-bearing complex, South Africa: evidence for sulfur contamination and multiple magma emplacements. Chem. Geol. 188, 149–159.

Li, C., Xu, Z., de Waal, S.A., Ripley, E.M., Maier, W.D., 2004. Compositional variations of olivine from the. Jinchuan Ni–Cu sulfide deposit, western China: implications for ore genesis Mineralium deposita 39 (2), 159–172.

Lightfoot, P.C., 2007. Advances in Ni–Cu–PGE deposit models and exploration technologies. In: Milkereit, B. (Ed.), Proceedings of Exploration 07: Fifth Decennial International Conference on Mineral Exploration, pp. 629–646.

Lightfoot, P.C., Evans-Lamswood, D., 2012. Magma chamber geometry and the localization of Ni–Cu +/-(PGE) sulfide mineralization: global examples and their relevance to Voisey's Bay. Diversity of Nickel Deposits in the WorldAEMQ, Quebec City (http://www.aemq.org/en/EVENEMENTS-CEMQ-2012_PROG_20NOV).

Lightfoot, P.C., Evans-Lamswood, D., 2013. Structural controls on Ni–Cu–PGE sulfide mineralization in the roots of large igneous provinces. PDAC, Toronto (http://convention.pdac.ca/pdac/conv/2013/pdf/ts/lip1-lightfoot.pdf).

Lightfoot, P.C., Evans-Lamswood, D., 2014. Near surface manifestations of the structural controls on Ni–Cu–PGE sulfide mineralization in the roots of large igneous provinces. Abstracts, GAC-MAC, Fredericton, p. 160.

Lightfoot, P.C., Farrow, C.E.G., 2003. Geology, geochemistry and mineralogy of the Worthington Offset Dyke: towards a genetic model for offset mineralization in the Sudbury Igneous Complex. Econ. Geol. 97, 1419–1446.

Lightfoot, P.C., Keays, R.R., 2005. Siderophile and chalcophile metal variations in flood basalts from the Siberian Trap, Noril'sk region: implications for the origin of the Ni–Cu–PGE sulfide ores. Econ. Geol. 100, 439–462.

Lightfoot, P.C., Naldrett, A.J., 1999. Geological and geochemical relationships in the Voisey's Bay intrusion Nain Plutonic Suite Labrador Canada, in Keays RR, Lesher CM, Lightfoot PC, and Farrow, CEG. Dynamic Processes in Magmatic Ore Deposits and Their Application in Mineral Exploration. Geol. Assoc. Can. 13, 1–31.

Lightfoot, P.C., Zotov, I.A., 2007. Ni–Cu–PGE sulfide deposits at Noril'sk, Russia. Third International Polar Year. PDAC, Toronto.

Lightfoot, P.C., Zotov, I.A., 2014. Geological Relationships between the intrusions, country rocks, and Ni–Cu–PGE sulfides of the Kharaelakh Intrusion, Noril'sk Region: implications for the roles of sulfide differentiation and metasomatism in their genesis. Northwest. Geol. 47, 1–35.

Lightfoot, P.C., Naldrett, A.J., Gorbachev, N.S., Doherty, W., Fedorenko, V.A., 1990. Geochemistry of the Siberian Trap of the Noril'sk Area, USSR, with implications for the relative contributions of crust and mantle to flood basalt magmatism. Contrib. Mineral. Petrol. 104, 631–644.

Lightfoot, P.C., Hawkesworth, C.J., Hergt, J., Naldrett, A.J., Gorbachev, N.S., Fedorenko, V.A., Doherty, W., 1993. Remobilisation of the continental lithosphere by mantle plumes: major-, trace-element, and Sr-, Nd-, and Pb-isotope evidence from picritic and tholeiitic lavas of the Noril'sk District, Siberian Trap, Russia. Contrib. Mineral. Petrol. 114, 171–188.

Lightfoot, P.C., Keays, R.R., Morrison, G.G., Bite, A., Farrell, K., 1997a. Geochemical relationships in the Sudbury Igneous Complex: Origin of the Main Mass and Offset Dikes. Econ. Geol. 92, 289–307.

Lightfoot, P.C., Keays, R.R., Morrison, G.G., Bite, A., Farrell, K., 1997b. Geologic and geochemical relationships between the contact sublayer, inclusions, and the main mass of the Sudbury Igneous Complex: a case study of the Whistle Mine Embayment. Econ. Geol. 92, 647–673.
Lightfoot, P.C., Keays, R.R., Evans-Lamswood, D.E., Wheeler, R., 2012a. S saturation history of Nain Plutonic Suite mafic intrusions: origin of the Voisey's Bay Ni–Cu–Co sulfide deposit, Labrador, Canada. Mineral. Deposita 47, 23–50.
Lightfoot, P.C., Evans-Lamswood, D., Wheeler, R., 2012b. The Voisey's Bay Ni–Cu–Co sulfide deposit, Labrador, Canada: emplacement of silicate and sulfide-laden magmas into spaces created within a structural corridor. Northwest. Geol. 45, 17–28.
Lightfoot, P.C., Stewart, R., Gribbin, G., Macek, J., Mooney, S., 2012c. Relative contribution of magmatic and post-magmatic processes in the genesis of the Thompson Belt Ni–Co sulfide ore deposits, Manitoba, Canada. International Conference on Nickel, Guiyang, China.
Lü, L.S., Mao, J.W., Li, H.B., Franco, P., Zhang, Z.H., Zhou, Z.H., 2011. Pyrrhotite Re–Os and SHRIMP zircon U–Pb dating of the Hongqiling Ni–Cu sulfide deposits in Northeast China. Ore Geol. Rev. 43, 106–119.
Maier, W.D., Groves, D.I., 2011. Temporal and spatial controls on the formation of magmatic PGE and Ni–Cu deposits. Miner. Deposita 46, 841–857.
Maier, W.D., Barnes, S.—J., Sarkar, A., Ripley, E., Li, C., Livesey, T., 2010. The Kabanga Ni sulfide deposit, Tanzania: I. Geology, petrography, silicate rock geochemistry, and sulfur and oxygen isotopes. Miner. Depos. 45, 419–441.
Maier, W.D., Gomwe, T., Barnes, S.-J., Li, C., Theart, H., 2004. Platinum group elements in the Uitkomst Complex, South Africa. Econ. Geol. 96, 499–516.
Malitch, K.N., Badanina, I.Yu., Belousova, E.A., Tuganova, E.V., 2012. Results of U–Pb dating of zircon and baddeleyite from the Noril'sk 1 ultramafic–mafic intrusion, Russia. Russ. Geol. Geophys. 53, 123–130.
Mann, P., 2007. Global catalogue, classification and tectonic origins of restraining- and releasing bends on active and ancient strike-slip fault systems. Geol. Soc. Lond. Spec. Publ. 290, 13–142.
Mao, J.W., Pirajno, F., Zhang, Z.H., Chai, F.M., Wu, H., Chen, S.P., Cheng, L.S., Yang, J.M., Zhang, C.Q., 2008. A review of the Cu–Ni sulfide deposits in the Chinese Tianshan and Altay orogens (Xinjiang Autonomous Region, NW China): principal characteristics and ore-forming processes. J. Asian Earth Sci. 32, 184–203.
Mezhvilk, A.A., 1984. The role of horizontal movements in the development of tectonic structures and deposits in the Noril'sk Region. Geotectonics 18, 70–78.
Mezhvilk, A.A., 2004. Thrust and strike-slip zones in Northern Russia. Geotectonics 28, 298–305.
Mungall, J.E., Harvey, J.D., Balch, S.J., Azar, B., Atkinson, J., Hamilton, M.A., 2010. Eagles' Nest: a magmatic ni-sulfide deposit in the James Bay Lowlands, Ontario, Canada. Econ. Geol. Spec. Publ. 15, 539–557.
Myers, J.S., Voordouw, R.J., Tettelaar, T.A., 2008. Proterozoic anorthosite–granite Nain batholith: structure and intrusion processes in an active lithosphere-scale fault zone, Northern Labrador. Can. J. Earth Sci. 45, 909–934.
Naldrett, A.J., 2004. Magmatic Sulfide Deposits. Springer. 727.
Naldrett, A.J., 2010. From the mantle to the bank: the life of a Ni–Cu–(PGE) sulfide deposit. S. Afr. J. Geol. 113, 1–32.
Naldrett, A.J., Li, C., 2007. The Voisey's Bay deposit, Labrador, Canada. In: Goodfellow, W.D. (Ed.), Mineral Deposits of Canada: A Synthesis of Major Deposit-Types. District Metallogeny, the Evolution of Geological Provinces, and Exploration Methods: Geological Association of Canada, Mineral Deposits Division, Sp Pub, 5, pp. 387–407.
Naldrett, A.J., Lightfoot, P.C., Fedorenko, V., Doherty, W., Gorbachev, N.S., 1992. Geology and geochemistry of intrusions and flood basalts of the Noril'sk region, USSR, with implications for the origin of the Ni–Cu ores. Econ. Geol. 87 (4), 975–1004.
Naldrett, A.J., Fedorenko, V.A., Lightfoot, P.C., Kunilov, V.E., Gorbachev, N.S., Doherty, W., Johan, Z., 1995. Ni–Cu–PGE deposits of the Noril'sk region Siberia: their formation in conduits for flood basalt volcanism. Trans. Inst. Min. Metall. 104, B18–B36.
Naldrett, A.J., Keats, H., Sparkes, K., Moore, R., 1996a. Geology of the Voisey's Bay Ni–Cu–Co deposit, Labrador, Canada. Explor. Min. Geol. 5, 169–179.
Naldrett, A.J., Fedorenko, V.A., Asif, M., Lin, Shushen, Kunilov, V.E., Stekhin, A.I., Lightfoot, P.C., Gorbachev, N.S., 1996b. Controls on the composition of Ni–Cu sulfide deposits as illustrated by those at Noril'sk Siberia. Econ. Geol. 91, 751–773.
Naldrett, A.J., Asif, M., Krstic, S., Li, C., 2000a. The composition of ore at the Voisey's Bay Ni–Cu sulfide deposit with special reference to platinum- group elements. Econ. Geol. 95, 845–866.
Naldrett, A.J., Singh, J., Krstic, S., Li, C., 2000b. The mineralogy of the Voisey's Bay Ni–Cu–Co deposit Northern Labrador Canada: influence of oxidation state on textures and mineral compositions. Econ. Geol. 95, 889–900.
Page, R.W., Hoatson, D.M., 2000. Geochronology of the mafic–ultramafic intrusions. In: Hoatson, D.M., Blake, D.H. (Eds.), Geology and economic potential of the Palaeoproterozoic layered mafic–ultramafic intrusions in the East Kimberley, Western Australia. Australian Geological Survey Organisation, Bulletin, 246, pp. 163–172.
Pirajno, F., 2012. The Geology and Tectonic Settings of China's Mineral Deposits. Springer.
Pu, C.J., Qin, D.X., Hian, H., Zhang, X., Pirajno, F., Fan, Z., 2007. Geological and geochemical characteristics of the Baimazhai Ni–Cu–(PGE) sulfide deposit in Yunnan, China. Chin. J. Geochem. 26, 374–383.
Ripley, E.M., Li, C., 2011. A review of conduit related Ni–Cu–(PGE) sulfide mineralization at the Voisey's Bay deposit, Labrador, and the Eagle deposit, northern Michigan. In: Li, C., Ripley, E.M. (Eds.), Magmatic Ni–Cu and PGE deposits: geology, geochemistry and genesis: reviews in economic geology, vol. 17. Society of Economic Geologists, Denver, Colorado, pp. 181–198.
Ryan, B., 1998. The Mesoproterozoic Nain Plutonic Suite in eastern Canada, and the setting of the Voisey's Bay Ni–Cu–Co sulfide deposit. Geosci. Can. 24, 173–188.
Ryan, B., 2000. The Nain–Churchill boundary and the Nain Plutonic Suite: a regional perspective on the geologic setting of the Voisey's Bay Ni–Cu–Co deposit. Econ. Geol. 95, 703–724.
Seat, Z., Beresford, S.W., Grguric, B.A., Waugh, R.S., Hronsky, J.M.A., Mary Gee, M.A., Groves, D.I., Mathison, C.I., 2007. Architecture and emplacement of the Nebo–Babel gabbronorite-hosted magmatic Ni–Cu–PGE sulfide deposit, West Musgrave, Western Australia. Miner. Deposita 42, 551–581.
Seat, Z., Beresford, S., Grguric, B.A., Gee, M.M.A., Grassineau, N.V., 2009. Reevaluation of the role of external sulfur addition in the genesis of Ni–Cu–PGE deposits: evidence from the Nebo–Babel Ni–Cu–PGE deposit, West Musgrave, Western Australia. Econ. Geol. 104, 521–538.
Shen, P., Shen, Y.C., Liu, T.B., Li, G.M., Zeng, Q.D., 2008. Prediction of hidden Au and Cu–Ni ores from depleted mines in Northwestern China: four case studies of integrated geological and geophysical investigations. Miner. Deposita 43, 499–517.
Smyk, M.C., Hollings, P., 2009. Mesoproterozoic midcontinent rift-related mafic intrusions near Thunder Bay: update. Summary of Field Work and Other Activities, 2009, Ontario Geological Survey, Open File Report 6240, pp. 11-1–11-5.
Song, X.Y., Zhou, M.-F., Cao, Z.M., Sun, M., Wang, Y.L., 2003. Ni–Cu–(PGE) magmatic sulfide deposits in the Yangliuping area, Permian Emeishan igneous province, SW China. Mineral. Deposita 38, 831–843.
Stekhin, A.I., 1994. Mineralogical and geochemical characteristics of the Cu–Ni ores of the Oktyabr'sky and Talnakh deposits. In: Lightfoot, P.C., Naldrett, A.J., Sheahan, P. (Eds.), Proceedings of the Sudbury-Noril'sk Symposium. Ontario Geological Survey, Special Publication, 5, pp. 217–230.
Sun, T., Qian, Z.Z., Li, C., Xia, M.Z., Yang, S.H., 2013. Petrogenesis and economic potential of the Erhongwa mafic–ultramafic intrusion in the Central Asian Orogenic Belt, NW China: constraints from olivine chemistry, U–Pb age and Hf isotopes of zircons, and whole-rock Sr–Nd–Pn isotopes. Lithos 182–183, 185–199.
Sutcliffe, R.H., 1987. Petrology of Middle Proterozoic diabases and picrites from Lake Nipigon, Canada. Contrib. Mineral. Petrol. 96, 201–211.
Tang, Z., 1992. Nickel deposit of China. Mineral Deposits of China, vol. 2. Beijing Publishing House, pp. 52–99 (Chapter 6).
Tang, Z., 1993. Genetic model of the Jinchuan nickel–copper deposit. In: Kirkham, R.V., Sinclair, W.D., Thorpe, R.I., Duke, J.M. (Eds.), Mineral deposit modelling. Geological Survey of Canada Special Paper, 40, pp. 389–401.
Thornett, J.R., 1981. The Sally Malay deposit: gabbroid associated nickel–copper sulfide mineralization in the Halls Creek Mobile Zone, Western Australia. Econ. Geol. 76, 1565–1580.
Upton, B.G.J., Blundell, D.J., 1978. The Gardar Igneous Province: evidence for proterozoic continental rifting. NATO Advanced Study Institute Series, 36, pp. 163–172.
Wang, R.M., Liu, D.Q., Yin, D.T., 1987. The conditions of controlling metallogeny of Cu, Ni sulfide ore deposits and the orientation of finding ore, Hami, Xinjiang, China. Miner. Rocks 3, 1–159 (Special Issue in Mandarin).
Wang, C.Y., Zhou, M.F., 2006. Genesis of the Permian Baimazhai magmatic Ni–Cu–(PGE) sulfide deposit, Yunnan, SW China. Mineral. Deposita 41, 771–783.
Wang, R., Zhao, C.L., et al., 1991. Kalatongke Cu–Ni Sulfide No. 1 ore deposit in Xinjiang. Geological Memoirs, Series 4, No 19. Beijing Geological Publishing House, pp. 1–319 (in Mandarin).
Wang, F.T., Ma, T.L., Liu, H.H., Li, Y.G., Hu, W.L., Zhao, C.L., Yuan, Q.L, Qi, F., 1992. Metallogeny and Prospecting Modelof the Karatungk Cu-Ni-Au ore belt in Xinjiang. People's Republic of China Ministry of Geology and Mineral Resources, Geological Memoirs Series 4, Number 23, 298.
Wang, C.Y., Zhou, M.F., Keays, R.R., 2006. Geochemical constraints on the origin of the Permian Baimazhai mafic–ultramafic intrusion, SW China. Contrib. Mineral. Petrol. 152, 309–321.
Wang, Y.W., Wang, J.B., Wang, L.J., Long, L.L., Liao, Z., Zhang, H.Q., Tang, P.Z., 2011. Problems of PGE metallogenesis related to mafic–ultramafic complexes in North Xinjiang, China. Geosci. Front. 2, 187–198.
Wang, C.Y., Zhou, M.F., Sun, Y., Arndt, N.T., 2012. Differentiation, crustal contamination and emplacement of magmas in the formation of the Nantianwan mafic intrusion of the ~260 Ma Emeishan large igneous province, SW China. Contrib. Mineral. Petrol. 164, 281–301.
Wang, D.C., Jahn, B.M., Shu, L., Chen, Y., Zhai, Y.Z., Branquet, Y., Barbanson, L., Sizaret, S., 2014. Late Paleozoic pre- and syn-kinematic plutons of the Kangguer–Huangshan Shear Zone; inference on the tectonic evolution of the eastern Chinese Tianshan. Am. J. Sci. 314, 43–79.
Wei, B., Wang, C.Y., Sun, C.L., 2013. Origin of PGE-depleted Ni–Cu sulfide mineralization in the Triassic Hongqiling No.7 orthopyroxenite intrusion, Central Asian Orogenic Belt, NE China. Econ. Geol. 108, 1813–1831.
Wilson, J.T., 1965. A new class of faults and their bearing on continental drift. Nature 207, 343–347.
Wu, F.Y., Wilde, S.A., Zhang, G.L., Sun, D.Y., 2004. Geochronology and petrogenesis of the post-orogenic Cu–Ni sulfide-bearing mafic–ultramafic complexes in Jilin Province, NE China. J. Asian Earth Sci. 23, 781–797.
Yakubchuk, A., Nikishin, A., 2004. Noril'sk–Talnakh Cu–Ni–PGE deposits: a revised tectonic model. Mineral. Deposita 39, 125–142.
Yang, S.-H., Zhou, M.-F., Lightfoot, P.C., Malpas, J., Qu, W.-J., Zhou, J.-B., Kong, D.-Y., 2012. Selective crustal contamination and decoupling of lithophile and chalcophile element isotopes in sulfide-bearing mafic intrusions: an example from the Jingbulake Intrusion, Xinjiang, NW China. Chem. Geol. 302–303, 106–118.
Zenko, T.E., Czamanske, G.K., 1994. Spatial and petrologic aspects of the intrusions of the Norilsk and Talnakh ore junctions. In: Naldrett, A.J., Lightfoot, P.C., Sheahan, P. (Eds.), The Sudbury–Norilsk Symposium Ontario Geological Survey Special Publication, 5, pp. 263–282.
Zhang, Y.X., Luo, Y.N., Yang, C.X., 1988. Panxi Rift and its geodynamics. Geological Memoirs, Ministry of Geology and Mineral Resources, Series 5, No 5.
Zhang, Z.H., Wang, Z.L., Mao, J.W., Cai, F.M., Yang, F.W., Yang, J.M., 2006. Geochemical character of the Jingbulake mafic complex, Western Tianshan. Acta Geol. Sin. 80, 1005–1016.

Zhou, M-F., Yang, Z-X., Song, X-Y., Keays, R.R., and Lesher, C.M.2002. Magmatic Ni–Cu–(PGE) Sulfide Deposits in China, in L.J. Cabri (Editor), The Geology, Geochemistry, Mineralogy, and Mineral Beneficiation of the Platinum-Group Elements, Edited by. Canadian Institute of Mining, Metallurgy and Petroleum, Special Volume 54, 619–636.

Zhou, M.F., Robinson, P.T., Lesher, C.M., Keays, R.R., Zhang, C.J., Malpas, J., 2005. Petrogenesis and metallogenesis of the Panzhihua gabbroic layered intrusion and associated Fe–Ti–V oxide deposits, Sichuan province, SW China. J. Petrol. 46, 2253–2280.

Zhu, F.L., Tao, Y., Hu, R.Z., Yu, S.Y., Qu, W.J., Du, A.D., 2011. Re–Os isotopic constraints on the ore-forming mechanism for the Qingkuangshan Ni–Cu–PGE deposit in the Huili County, Sichuan Province. Acta Petrol. Sin. 27 (9), 2655–2664 (In Mandarin).

Zotov, I.A., 1989. Transmagmatic fluids in magmatism and ore formation. Nauka, Moscow (256 pp. In Russian).